HHS Public Access

Author manuscript

Nature. Author manuscript; available in PMC 2021 October 07.

Published in final edited form as:

Nature. 2020 October ; 586(7829): 434–439. doi:10.1038/s41586-020-2799-2.

A STAT3 palmitoylation cycle promotes T_H17 differentiation and colitis

Mingming Zhang[1,2], **Lixing Zhou**[3], **Yuejie Xu**[4], **Min Yang**[2], **Yilai Xu**[2], **Garrison Paul Komaniecki**[2], **Tatsiana Kosciuk**[2], **Xiao Chen**[2], **Xuan Lu**[2], **Xiaoping Zou**[4], **Maurine E. Linder**[5], **Hening Lin**[1,2,†]

[1]Howard Hughes Medical Institute, Department of Chemistry and Chemical Biology, Cornell University, Ithaca, NY, USA.

[2]Department of Chemistry and Chemical Biology, Cornell University, Ithaca, NY, USA.

[3]The Center of Gerontology and Geriatrics/National Clinical Research Center for Geriatrics, West China Hospital, Sichuan University, Chengdu, China.

[4]Department of Gastroenterology, Nanjing Drum Tower Hospital, the Affiliated Hospital of Nanjing University Medical School, Nanjing University, Nanjing, China.

[5]Department of Molecular Medicine, Cornell University, Ithaca, NY, USA.

Abstract

Cysteine palmitoylation (S-palmitoylation) is a reversible post-translational modification that is installed by the DHHC family of palmitoyltransferases and is reversed by several acyl protein thioesterases[1,2]. Although thousands of human proteins are known to undergo S-palmitoylation, how this modification is regulated to modulate specific biological functions is poorly understood. Here we report that the key T helper 17 (T_H17) cell differentiation stimulator, STAT3[3,4], is subject to reversible S-palmitoylation on cysteine 108. DHHC7 palmitoylates STAT3 and promotes its membrane recruitment and phosphorylation. Acyl protein thioesterase 2 (APT2, also known as LYPLA2) depalmitoylates the phosphorylated STAT3 (p-STAT3) and enables it to translocate to the nucleus. This palmitoylation–depalmitoylation cycle enhances STAT3 activation and promotes T_H17 cell differentiation; perturbation of either palmitoylation or depalmitoylation negatively affects T_H17 cell differentiation. Overactivation of T_H17 cells is associated with several inflammatory diseases, including inflammatory bowel disease (IBD). In a mouse model, pharmacological inhibition of APT2 or knockout of *Zdhhc7*—which encodes DHHC7 [Author: OK?]—relieves the symptoms of IBD. Our study reveals not only a potential therapeutic strategy for the treatment of IBD but also a model through which S-palmitoylation regulates cell signalling,

[†]**Correspondence and requests for materials** should be addressed to H.L. hl379@cornell.edu.

Author contributions M.Z. and H.L. designed the study; M.Z. carried out the cell experiments and the protein analysis; M.Z. and X.C. performed the click chemistry analysis; L.Z. [Author: Please clarify which author this refers to, as there seems to be no one with these initials in the author list. Should this be L.Z.?] and Yuejie Xu collected the human samples and performed the analyses; M.Y. carried out the chemical synthesis; Yilai Xu [Author: Is this Yilai Xu?], G.P.K. and T.K. repeated key cellular biochemical experiments with both DHHC7 and APT2; X.L. and M.Z. carried out the mouse experiments; M.Z. [Author: Please clarify which author this refers to; should this be M.Z.?] and H.L. drafted the manuscript with inputs from all authors; X.Z. directed the patient study; M.E.L. provided all of the DHHC plasmids and participated in data analysis; and H.L. directed the biochemical studies. All authors read and approved the final manuscript.

Competing interests The authors declare no competing interests.

which might be broadly applicable for understanding the signalling functions of numerous S-palmitoylation events.

IBD—which includes ulcerative colitis and Crohn's disease—is a chronic inflammatory disease for which treatments are limited[4]. Although the aetiology of IBD is unknown, the association between IBD and immune dysregulation has been extensively studied[4]. The abundance of proinflammatory cells in patients with IBD contributes to its progression, and blocking the differentiation of proinflammatory cells could be useful in treatment of the disease[5].

T_H17 cells are a subgroup of proinflammatory T cells that are characterized by the expression of interleukin-17 (IL-17, encoded by *IL17A*) and retinoic acid receptor-related orphan receptor gamma t (RORγt, encoded by *RORC*)[6]. Accelerated differentiation of T_H17 cells has an important pathogenic role in IBD, and the abundance of T_H17 cells correlates with disease activity in mouse models of IBD and in patients[7]. The serum of patients with IBD is rich in cytokines, enabling the differentiation of T_H17 from naive $CD4^+$ T cells[5]. Under specific cytokine stimulation, STAT3 in naive $CD4^+$ T cells is phosphorylated by Janus kinase 2 (JAK2)[3]. As a key transcription factor, p-STAT3 promotes the expression of downstream target genes (*RORC* and *IL17A*) and the differentiation of T_H17 cells[3,4,7].

Owing to the important role of STAT3 in T_H17 differentiation, understanding how STAT3 is regulated could provide new ways to control T_H17 and therefore IBD. We became interested in the regulation of STAT3 by post-translational modifications, in particular protein cysteine palmitoylation. S-palmitoylation has emerged as an important post-translational modification that regulates protein membrane association and protein–protein interactions[1,2]. S-palmitoylation is catalysed by 23 mammalian palmitoyltransferases—known as DHHCs because of the conserved Asp-His-His-Cys sequence motif[2]—and is removed by acyl protein thioesterases (APT1, APT2 and ABHD family members)[8]. Although both DHHCs and APTs are known to act on numerous proteins[1], the physiological function of palmitoylation remains unclear, and how DHHCs and APTs affect T_H17 cell differentiation has not been reported.

Here we show that STAT3 undergoes reversible S-palmitoylation on Cys108, catalysed by DHHC7 and APT2 (encoded by *LYPLA2*). We describe an active directional palmitoylation–depalmitoylation cycle for STAT3, which is driven by the ability of APT2 to selectively depalmitoylate p-STAT3. This palmitoylation–depalmitoylation cycle promotes T_H17 cell differentiation by promoting the membrane association, phosphorylation and nuclear translocation of STAT3. Interruption of the palmitoylation–depalmitoylation cycle by DHHC7 knockout or through the inhibition of APT2 relieves the symptoms of colitis in a mouse model, thus revealing a potential therapeutic strategy for the treatment of IBD.

STAT3 is palmitoylated by DHHC7

Recruitment of STAT3 to the plasma membrane is essential for its phosphorylation[3]. We first inquired whether S-palmitoylation would contribute to the membrane association of STAT3. Although the S-palmitoylation of STAT3 was reported while our manuscript was in

preparation[9], the findings we present here differ from the results of that study, which has since been retracted.

In order to visualize STAT3 palmitoylation in the presence of mouse DHHCs in HEK293T cells, we used the alkyne-tagged palmitic acid analogue Alk14 as a metabolic label, which can conjugate with the fluorescent dye TAMRA azide via click chemistry. DHHC7 (encoded by *Zdhhc7*) and DHHC3 (encoded by *Zdhhc3*) increased the palmitoylation level of STAT3 (Extended Data Fig. 1a, b). Quantification revealed that STAT3 palmitoylation increased 5.4-fold upon DHHC7 expression (Extended Data Fig. 1c); the effect of DHHC3 was weaker. Palmitoylation can occur on cysteine or lysine residues (on sulfur or nitrogen, respectively), but only S-palmitoylation is sensitive to hydroxylamine[10]. Treatment with hydroxylamine removed more than 90% of the palmitoylation signal on STAT3, suggesting that palmitoylation of STAT3 by DHHC7 primarily occurred on cysteine (Fig. 1a).

To confirm that DHHC7 is the endogenous STAT3 palmitoyltransferase, we generated DHHC7-knockout HEK293T cells and mouse splenocytes. S-palmitoylation of STAT3 in DHHC7-knockout cells was significantly decreased compared with control cells (Extended Data Fig. 2a–d). Re-expression of wild-type DHHC7—but not of the catalytically inactive DHHS7 mutant, containing a cysteine-to-serine substitution in the conserved motif—significantly increased STAT3 palmitoylation (Extended Data Fig. 2b). We further confirmed DHHC7-promoted STAT3 palmitoylation using an acyl–biotin exchange assay (Extended Data Fig. 2e), another commonly used method to detect S-palmitoylation.

Given the previous report that human DHHC19 acts as the palmitoyltransferase for STAT3, [9] we considered whether sequence differences between human and mouse DHHCs could account for the difference in findings. We tested human DHHC3, DHHC7 and DHHC19, and found that human DHHC7 is the most efficient STAT3 palmitoyltransferase (Extended Data Fig. 2f).

There are seven members in the STAT family, of which STAT1 is the most similar to STAT3[11]. Using an acyl–biotin exchange assay, we showed that STAT1 is also palmitoylated; however, its palmitoylation levels were not increased in the presence of DHHC7 (Extended Data Fig. 2g).

Palmitoylation targets STAT3 to membranes

To map the palmitoylation site of STAT3, we individually mutated each of the 14 cysteine residues of STAT3 to serine and examined the palmitoylation status of the mutants. The palmitoylation signal of STAT3 showed a notable decrease only when Cys108 was mutated (Extended Data Fig. 3a–d). Notably, the interaction between STAT3(C108S) and DHHC7 also decreased compared with that involving wild-type STAT3 (Extended Data Fig. 3a). Overexpression of neither DHHC7 nor DHHC3 could increase the palmitoylation of STAT3(C108S) (Extended Data Fig. 3b, e).

Because S-palmitoylation can target proteins to membranes[1], and STAT3 needs to be recruited to the plasma membrane in order to interact with JAK2[3], we next examined whether S-palmitoylation affects STAT3 membrane recruitment. Wild-type STAT3 was

localized at the plasma membrane, on endomembranes, and in the nucleus. Knockout of DHHC7 in HEK293T cells decreased the membrane localization of STAT3 but increased its nuclear localization (Fig. 1b, Extended Data Fig. 4a, b). Consistent with this, STAT3(C108S) was found prominently in the nucleus (Extended Data Fig. 4c), suggesting that palmitoylation promotes the membrane localization of STAT3. Furthermore, the re-expression of DHHC7 in DHHC7-knockout HEK293T cells led to the membrane recruitment of wild-type STAT3 but not of STAT3(C108S) (Fig. 1c, Extended Data Fig. 4d). In both HEK293T cells and mouse splenocytes, DHHC7 induced palmitoylation of STAT3 and increased the amount of the modified protein in the membrane but not in the nuclear fractions (Fig. 1d, Extended Data Fig. 4e). Endogenous STAT3 co-localized to a greater extent with JAK2 in wild-type than in DHHC7-knockout cells (Fig. 1b), Collectively, the results suggest that DHHC7-catalysed palmitoylation promotes the membrane localization of STAT3 and its interaction with JAK2.

DHHC7 promotes STAT3 activation

The transcriptional activity of STAT3 is dependent on its phosphorylation at Y705[3,12]. We next examined whether palmitoylation could facilitate STAT3 phosphorylation. Consistent with the palmitoylation screen (Extended Data Fig. 1), STAT3 phosphorylation was notably (and selectively) increased by the expression of DHHC7 or DHHC3, with DHHC7 being the more effective (Extended Data Fig. 5). Endogenous STAT3 phosphorylation was regulated similarly by DHHC7 expression in both HEK293T cells and mouse splenocytes (Extended Data Fig. 6a, b). DHHC7 knockout in HEK293T cells decreased the phosphorylation of endogenous wild-type STAT3 (Extended Data Fig. 6c), but not of the ectopically expressed mutant STAT3(C108S) (Extended Data Fig. 6d). We therefore concluded that DHHC7 regulates STAT3 phosphorylation.

We next co-expressed DHHC7 with wild-type STAT3, STAT3(C108S) and STAT3(Y705F). Phosphorylation of STAT3(C108S) was reduced relative to that of wild-type STAT3, whereas the palmitoylation status of STAT3 was unaffected by mutation of the Y705 phosphorylation site (Fig. 2a). Thus, STAT3 phosphorylation is facilitated by palmitoylation, but phosphorylation does not affect palmitoylation by DHHC7.

Subcellular fractionation showed that DHHC7 increased the membrane recruitment of STAT3 (Extended Data Fig. 4b) as well as the p-STAT3 signal located on membranes and in the nucleus (Extended Data Fig. 6e). Notably, the ratio of p-STAT3 to STAT3 was increased by DHHC7 only in the nuclear fraction (Extended Data Fig. 6e). The membrane recruitment and phosphorylation of STAT3(C108S) was reduced relative to that of wild-type STAT3 (Fig. 2b). Similarly, immunofluorescence imaging showed that, in DHHC7-expressing cells, wild-type STAT3 was more extensively located at the plasma membrane and endomembrane and had higher phosphorylation levels compared with STAT3(C108S), which was localized mainly in the nucleus (Fig. 2c, Extended Data Fig. 6f). These data additionally support that the palmitoylation of STAT3 facilitates its phosphorylation by promoting its recruitment to the membrane, where JAK2 kinase is localized.

APT2 depalmitoylates p-STAT3

APTs are involved in regulating the membrane localization of target proteins by depalmitoylation[13]. Both APT1 and APT2 can be palmitoylated on Cys2, which promotes their membrane localization and access to substrates in membranes[14]. It has recently been shown that APT1 is mainly localized in the mitochondria[15]. We therefore focused on testing whether STAT3 is a substrate of APT2. Haemagglutinin (HA)-tagged STAT3 and Flag-tagged APT2 were found to associate with each other in HEK293T cells. Wild-type APT2 interacted with STAT3 more strongly than did the mutant APT2(C2S) (Extended Data Fig. 7a). Expression of APT2 decreased the STAT3 palmitoylation signal (Fig. 2d, e, Extended Data Fig. 7b). The C2S mutant or the catalytically inactive S122A mutant of APT2 failed to decrease the palmitoylation signal of STAT3 (Fig. 2d, Extended Data Fig. 7, c). APT2 knockdown and pharmacological inhibition of APT2 with ML349[16] also increased STAT3 palmitoylation (Fig. 2f, Extended Data Fig. 7d). These results indicate that APT2 can depalmitoylate STAT3.

We next evaluated whether depalmitoylation by APT2 regulates STAT3 phosphorylation and transcriptional activity. Given that DHHC7-catalysed palmitoylation promotes STAT3 activity, we expected that STAT3 activity would be increased upon APT2 knockdown. However, APT2 knockdown inhibited both the transcriptional activity of STAT3 (Extended Data Fig. 7e, f) and its nuclear translocation (Fig. 2g). Furthermore, co-expression of wild-type DHHC7 and APT2 promoted the expression of downstream genes to a greater extent than their mutant counterparts (Extended Data Fig. 7g). The dimerization of STAT3 is reported to be important for its transcriptional activity and is regulated by various post-translational modifications[9,17]; however, it was affected by palmitoylation (Extended Data Fig. 7h).

To explain the finding that both palmitoylation and depalmitoylation promote STAT3 signalling, we suggest that depalmitoylation of STAT3 occurs mainly on p-STAT3—serving to release p-STAT3 from membranes to promote its nuclear translocation. To test this hypothesis, we generated the HA-tagged phosphorylation site mutant STAT3(Y705F) and repeated the STAT3–APT2 interaction experiment. Compared with wild-type STAT3, the association between STAT3(Y705F) and APT2 was reduced (Extended Data Fig. 7i). Consistent with the results of the physical interaction studies, depalmitoylation of STAT3(Y705F) by APT2 was much less efficient (Fig. 2e, Extended Data Fig. 7b). When JAK2 was inhibited with fedratinib, phosphorylation of STAT3 decreased as expected; however, levels of membrane-localized STAT3 increased whereas those of nuclear STAT3 decreased (Fig. 2h). Collectively, the data support the hypothesis that APT2 preferentially promotes the depalmitoylation and nuclear translocation of p-STAT3 over STAT3.

STAT3 palmitoylation cycle promotes T_H17

Because STAT3 is important for T_H17 cell differentiation, we evaluated whether the palmitoylation–depalmitoylation cycle of STAT3 promotes the generation of T_H17 cells from mouse spleen cells[7]. Under T_H17 differentiation conditions, STAT3 phosphorylation and transcriptional activity were promoted to a greater extent when STAT3 was co-expressed

with wild-type DHHC7 than with inactive DHHS7 (Fig. 3a, Extended Data Fig. 8a–e). These results were further confirmed by quantification of T_H17 cells using flow cytometry (Fig. 3b, Extended Data Fig. 8f). Inhibition of APT2 by ML349 significantly decreased the expression of STAT3 target genes (*RORC* and *CCND1*) and the differentiation of T_H17 cells (Fig. 3c, Extended Data Fig. 8g). *Zdhhc7* knockout also decreased T_H17 cell differentiation (Fig. 3d) and STAT3 phosphorylation (Fig. 3e). The palmitoylation–depalmitoylation cycle is therefore important for STAT3 signalling and T_H17 differentiation.

DHHC7 and APT2 are upregulated in patients with IBD

Activated STAT3 is suggestive of a poor prognosis in various autoimmune diseases[18], and the level of T_H17 cells is a key factor that affects the course and severity of intestinal inflammation[19]. To determine whether expression levels of *ZDHHC7* and *LYPLA2*—genes that promote the palmitoylation–depalmitoylation cycle—are correlated with intestinal inflammation in humans, human peripheral blood mononuclear cells (PBMCs) from 26 healthy participants, 24 patients with Crohn's disease and 10 patients with ulcerative colitis were extracted and analysed. *ZDHHC7* and *LYPLA2* mRNA was upregulated in patients with IBD, especially those with ulcerative colitis (Fig. 4a). Downstream target genes of STAT3—*RORC* and *IL17A*—were also highly expressed (Extended Data Fig. 9a). In addition, cells from individuals with more active IBD show higher expression levels of *ZDHHC7*, *LYPLA2*, *RORC* and *IL17A* (Fig. 4b, Extended Data Fig. 9b). There was a significant correlation between the expression of the STAT3 target genes (*RORC* and *IL17A*) and that of *ZDHHC7* and *LYPLA2* (Fig. 4c, Extended Data Fig. 9c–h). Furthermore, p-STAT3 levels correlated with levels of *ZDHHC7* and *LYPLA2* mRNA in PBMCs (Fig. 4d). Notably, *ZDHHC7* mRNA levels correlated with those of STAT3 target genes—as well as levels of p-STAT3—only in patients with IBD, whereas mRNA levels of *LYPLA2* and STAT3 target genes showed excellent correlation in both healthy participants and in patients with IBD (Fig. 4c, d, Extended Data Fig. 9c–h). These results suggest that changes in the expression of *LYPLA2* might be more relevant for IBD. The expression of *ZDHHC7* correlated less well with that of STAT3 target genes—probably because DHHC3 could also regulate STAT3, as our early data indicate. Consistent with this hypothesis, *ZDHHC3* expression levels were also increased in patients with IBD compared with healthy participants (Extended Data Fig. 9a).

Targeting APT2 or DHHC7 reduces colitis in mice

We tested whether the pharmacological inhibition of APT2 with ML349 could reduce dextran sulfate sodium (DSS)-induced colitis in mice, an experimental model for IBD. ML349 (50 mg kg^{-1}) was well tolerated by the mice (Extended Data Fig. 10a). In the DSS-induced mouse model of colitis, pretreatment with ML349 followed by treatment with DSS significantly attenuated weight loss and increased the survival rate (Extended Data Fig. 10b, c)—indicating that ML349 treatment could effectively prevent DSS-induced colitis. DSS treatment followed by ML349 treatment also significantly attenuated weight loss and colon shortening in mice (Fig. 4e, Extended Data Fig. 10d, e), indicating that ML349 could alleviate DSS-induced colitis. Furthermore, consistent with the in vitro results (Fig. 3), ML349 significantly decreased the levels of T_H17 cells in mouse splenocytes (Fig. 4f).

To provide additional support for these findings, we also used *Zdhhc7*-knockout mice in the colitis model. On the basis of our mechanistic model (Fig. 4i), we predicted that knockout of *Zdhhc7* should also reduce DSS-induced colitis. Indeed, we found that *Zdhhc7* knockout decreased T_H17 cell differentiation and protected mice from DSS-induced colitis (Fig. 4g, h, Extended Data Fig. 10f). We therefore suggest that the STAT3 palmitoylation–depalmitoylation cycle could be a promising therapeutic target for T_H17-related immune disorders.

Discussion

The transcription factor STAT3 is known to be recruited to the plasma membrane and phosphorylated by JAK2 under specific stimulation. p-STAT3 then migrates to the nucleus and promotes the expression of target genes[3,12]. However, very little is known about the mechanism by which STAT3 is recruited to the membrane. Here we showed that Cys108 of STAT3 is palmitoylated by DHHC7 (and to a lesser extent by DHHC3), which promotes membrane recruitment and phosphorylation by JAK2. Although palmitoylation is well known to be important for membrane distribution and signalling outputs[1,2], how palmitoylation and depalmitoyation are balanced to promote signalling has been a fundamental unaddressed question. Palmitoylation anchors STAT3 to the cell membranes, but for nuclear translocation, it must be depalmitoylated. We showed that APT2 contributes to the nuclear translocation of p-STAT3 by selectively depalmitoylating p-STAT3 over unphosphorylated STAT3. These results suggest a model in which the palmitoylation–depalmitoylation cycle, rather than being a futile cycle, drives STAT3 activation (Fig. 4i). Without this cycle, even though STAT3 can still form homodimers and translocate to the nucleus, most STAT3 is present in its inactive unphosphorylated state (Fig. 4i).

Constitutive activation of STAT3 contributes to T_H17 differentiation in patients with immune disorders, leading to poor clinical outcomes[7,12]. STAT3 has been proven to be an effective target for inhibiting T_H17 cell differentiation and attenuating colitis in mouse models of IBD[7]. Our work demonstrates that the palmitoylation–depalmitoylation cycle of STAT3 affects T_H17 cell differentiation, and suggests that both DHHC7 and APT2 could be new therapeutic targets for treating colitis. Because T_H17 cells are a key factor affecting the course and severity of various immune disorders such as IBD, hyper-IgE syndrome and arthritis[12,19,20], the palmitoylation–depalmitoylation cycle of STAT3 could be a potential therapeutic target for the treatment of many other autoimmune disorders.

Post-translational modifications are particularly suited for mediating cell signalling, as evidenced by the well-known signalling functions of phosphorylation and ubiquitination. Protein S-palmitoylation was discovered as a post-translational modification several decades ago[21], yet despite the fact that close to 3,000 proteins in humans are known to undergo this modification, very little is understood about how it contributes to cell signalling [1]. This study demonstrates that a palmitoylation–depalmitoylation cycle can proceed in a specific direction to promote cell signalling, with the direction of the cycle in this case ensured by the specificity of APT2 towards the phosphorylated substrate. This example could provide important insights for understanding the signalling functions of S-palmitoylation in numerous other cell signalling processes.

METHODS

Ethics approval

The protocols for collection of human PBMCs from healthy participants in the study were approved by the Ethical Committee of Drum Tower Hospital, Nanjing University. All of the participants provided informed consent. This study was performed in compliance with all relevant ethical regulations. Control subjects were healthy volunteers or had non-inflammatory disorders (constipation, reflux, non-ulcer dyspepsia, etc.). The diagnosis of IBD was based on clinical, endoscopic and histological criteria. Disease activity was assessed using the Crohn's disease activity index[23] for Crohn's disease and the simple clinical colitis activity index score[24] for ulcerative colitis. The baseline characteristics of all participants are shown in Supplementary Table 1.

Zdhhc7-knockout mice

The mouse strain used for this research project, B6.129P2(FVB)-Zdhhc7tm1.2Lusc/Mmmh, RRID:MMRRC_043511-MU, was obtained from the Mutant Mouse Resource and Research Center (MMRRC) at the University of Missouri, an NIH-funded strain repository, and was donated to the MMRRC by B. Luscher (The Pennsylvania State University). Genotype identification was performed according to the MMRRC protocol. Primers for the wild-type allele were as follows: forward: TGAGCCAGGATGGATTTCAGACA and reverse: TGCCCTCGGACGCAGGAGATGAA. Primers for the mutant type allele were as follows: forward: TCCCCTGATGTATGCGAATGTCC and reverse: AACAGGTGCCTTTTGAATGTCAG.

DSS-induced mouse colitis model

The mouse protocol 2019–0009 was approved by the Institutional Animal Care and Use Committee (IACUC) at Cornell University. All animals were housed under specific-pathogen-free conditions following the regulations of the IACUC. Mice (6–8 weeks old) were randomized into different groups (8 mice per group, mixed sex) as indicated. Colitis was induced by treating with 3.0% DSS (MP Biomedicals) in their drinking water ad libitum. ML349 (synthesized by our laboratory) solution was intraperitoneally injected into the mice at the indicated doses every other day. All mice were euthanized and the spleens were isolated to detect T cells. The distance from caecum to anus was measured. The colon was fixed in 4% paraformaldehyde for pathological examination. The study was not blinded.

Common reagents and antibodies

The following reagents and antibodies were purchased from commercial sources: inhibitor cocktail (Trichostatin A (TSA, T8552, Sigma), protease inhibitor cocktail (P8340, Sigma), phosphatase inhibitor cocktail (P0044, Sigma)), fedratinib (S2736, Selleckchem), universal nuclease (88700, Thermo Fisher), Bradford assay (23200, Thermo Fisher), dithiothreitol (DTT; DTT100, Goldbio), enzyme-linked chemiluminescence (ECL) plus (32132, Thermo Fisher), SYBR Green PCR Master Mix (4472908, Applied Biosystems), streptavidin agarose (20359, Thermo Fisher), Protein A/G PLUS-Agarose (sc-2003, Santa Cruz Biotechnology), anti-Flag agarose gel (A2220, Sigma) and anti-HA affinity gel (E6779,

Sigma). Antibodies were as follows: STAT3 (9139, CST), phospho-STAT3 (Tyr705) (ab76315, Abcam), β-actin (C4) HRP (SC-47778, Santa Cruz), Na/K-ATPase (SC-21712, Santa Cruz), histone H3 (4499S, CST), Flag HRP (A8592, Millipore), HA-probe (Y-11) (SC805, Santa Cruz), HA-probe (F-7) (SC7392, Santa Cruz), DHHC7 (ab138210, Abcam), DHHC7 (R12–3691, Assay Biotechnology), Alexa Fluor 350 goat anti-rabbit IgG (A-11046, Invitrogen), Alexa Fluor 594 goat anti-mouse IgG (8890S, CST), mouse CD4 PerCP-Cy5.5 (560767, BD Pharmingen), mouse IL-17A PE (560767, BD Pharmingen), anti-mouse IgG HRP (7076S, CST) and anti-rabbit IgG HRP (7074S, CST).

Cloning and mutagenesis

APT2 and DHHC1–23 murine plasmids were provided by M. Fukata. DHHC3/7/19 human plasmids were obtained from GenScript. STAT3 expression vectors with different tags were obtained from Addgene. Point mutations of plasmids were generated by QuikChange site-directed mutagenesis[25].

Cell culture and transfection

Human HEK293T cells (obtained from ATCC) were grown in DMEM media (11965–092, Gibco) with 10% bovine calf serum (CS, 12133C, Sigma) and extra 5% fetal bovine serum (FBS, 26140079, Gibco) to improve cell growth. *ZDHHC7*-knockout HEK293T cells were generated as previously described[26]. In brief, design of the guide RNA (gRNA) was carried out using the CRISPR Design Tool (http://crispr.mit.edu) to minimize potential off-target effects. Three pairs of gRNA sequences (#1, 5′-caccgGAGGATGATGCTCGACGTCC-3′, 5′-aaacGGACGTCGAGCATCATCCTCc-3′; #2, 5′-caccgCGTCGAGCATCATCCTCTCC-3′, 5′-aaacGGAGAGGATGATGCTCGACGc-3′; #3, 5′-caccgCGGGTCTGGTTCATCCGTGA-3′, 5′-aaacTCACGGATGAACCAGACCCGc-3′) were cloned in lentiCRISPR v2 vector (49535, Addgene) to generate *ZDHHC7*-targeting vectors. Then the targeting vector was transfected into HEK293T cells with FuGene 6 (E2691, Promega). The empty lentiCRISPR v2 vector was taken as control. Puromycin (2 μg ml^{-1}; P-600–100, GoldBio) was added in culture media after transfection for 24 h and cells were seeded as a single cell in each well of 96-well plates using a limited dilution method. Knockout of *ZDHHC7* was confirmed by western blot and three independent strains of monoclonal *ZDHHC7* knockout cell lines were selected for further experiments.

Splenocytes were isolated from mice by classic methods[7]. In brief, the excised spleen was sliced into small pieces and placed onto a strainer (352350, Thermo Fisher) attached to a 50 ml conical tube. The sliced spleen was pressed through the strainer using the plunger end of a syringe and the cells were washed through the strainer with excess 4 °C PBS. The cell suspension was centrifuged at 500*g* for 5 min at 4 °C. The cell pellet was suspended in 2 ml of red blood cell lysing buffer (R7757, Sigma) for 5 min at RT and diluted with 30 ml PBS. The cells were centrifuged at 500*g* for 5 min at RT. The cell pellet was suspended in 20 ml of 37 °C DMEM media, mixed well with 10 ml of Percoll density gradient media (17089102, VWR) and centrifuged at 2,500*g* for 5 min at RT. The collected cells were seeded in 37 °C RPMI 1640 medium (12633012, Gibco) supplemented with 10% FBS at 5 × 10^6 cells per ml. Splenocytes were cultured under T_H17-polarizing conditions: 3 ng ml^{-1}

TGF-β (100–21, PeproTech), 40 ng ml^{-1} IL-6 (200–06, PeproTech), 30 ng ml^{-1} IL-23 (200–23, PeproTech), 20 ng ml^{-1} tumour necrosis factor (TNF) (300–01A, PeproTech) and 10 ng ml^{-1} IL-1β (200–01B, PeproTech).

For HEK293T cells, the transient transfection was performed using FuGene 6 (E2691, Promega) or polyethylenimine (PEI) (24765, Polysciences). For splenocytes, the transient transfection was done using the Gene Pulser Xcell system with the recommended buffer (1652677, Bio-Rad) according to the manufacturer's protocol. *LYPLA2* knockdown was performed with siRNA (136366, Thermo Fisher).

Click chemistry and in-gel fluorescence detection

Cells were treated with 50 μM palmitic acid analogue Alkyne 14 (Alk14) for 5 h and the collected and lysed in 1% NP-40 lysis buffer (25 mM Tris-HCl pH 8.0, 150 mM NaCl, 10% glycerol, 1% Nonidet P-40) with protease inhibitor cocktail. The supernatant was collected after centrifugation at 16,000*g* for 20 min at 4 °C. The protein concentration was determined by Bradford assay (23200, Thermo Fisher). The target protein was purified with anti-Flag agarose beads and the beads were suspended in 50 μl of IP washing buffer. Click chemistry reagents were added to the beads in the following order: 1 μL of 4 mM TAMRA azide (47130, Lumiprobe), 1.2 μl of 10 mM tris[(1-benzyl-1*H*-1,2,3-triazol-4-yl)methyl]amine, (TBTA) (T2993, Tcichemicals), 1 μl of 40 mM $CuSO_4$, 1 μl of 40 mM tris(2-carboxyethyl)phosphine HCl (TCEP hydrochloride) (580560, Millipore). The reaction mixtures were mixed thoroughly and incubated for 30 min in the dark at room temperature. Then, 20 μl of 6×-SDS loading buffer was added and the resulting mixture was heated at 95 °C for 10 min. Half of the mixture was also treated with hydroxylamine (438227, Sigma) (pH 7.4, final concentration 500 μM) and heated for another 5 min at 95 °C to remove S-palmitoylation. The samples were then resolved by SDS–PAGE. For the overexpressed samples with high STAT3 levels, the gel was incubated with destaining buffer (50% CH_3OH, 40% water and 10% acetic acid) by shaking for 2–8 h at 4 °C and then incubated in water, which helped to lower the background. Otherwise, the gel was washed briefly in water. The gel was scanned to record the rhodamine fluorescence signal using a Typhoon 7000 Variable Mode Imager (GE Healthcare Life Sciences). After scanning, the gel was stained with Coomassie Brilliant Blue (B7920, Sigma) to check for protein loading.

Acyl–biotin exchange

Acyl–biotin exchange (ABE) assays were performed essentially as described previously[27]. Samples were suspended in 1 ml lysis buffer (100 mM Tris-HCl pH 7.2, 5 mM EDTA, 150 mM NaCl, 2.5% SDS, inhibitor cocktail) with 50 mM *N*-ethylmaleimide (NEM) (E3876, Sigma) and 50 U ml^{-1} nuclease (88700, Thermo Fisher). Samples were solubilized at room temperature (RT) for 2 h with gentle mixing and centrifuged at 16,000 g for 20 min. The protein concentration of the supernatant was determined using a Bradford assay. Protein (2 μg) for each sample was precipitated with chloroform/methanol/water (v/v 1:4:3), briefly air-dried, and dissolved in 1 ml of lysis buffer with 5 mM biotin-HPDP (16459, Cayman Chemical) by gentle mixing at RT. Samples were then equally divided into two parts and incubated with 0.5 ml of 1 M hydroxylamine or negative control (1 M NaCl) respectively at RT for 3 h. Samples were precipitated again and dissolved in 200 μl of resuspension buffer

(100 mM Tris-HCl pH 7.2, 2% SDS, 8 M urea, 5 mM EDTA). For each sample, 20 μl was used as loading control and 180 μl was diluted 1:10 with PBS and incubated with 20 μl of streptavidin beads with shaking overnight at 4 °C. Beads were washed 3 times with PBS containing 1% SDS. The beads and loading controls were mixed with SDS loading buffer and heated at 95 °C for 10 min. Samples were then resolved by SDS–PAGE and subjected to western blot analyses.

Western blot

Cells were lysed with 1% NP40 lysis buffer and proteins were blotted following a standard protocol. Signals were detected using the chemiluminescence of ECL plus (32132, Thermo Fisher) on a Typhoon scanner.

Subcellular fractionation

Cells were collected and suspended in subcellular fraction buffer (250 mM sucrose, 20 mM HEPES, pH 7.4, 10 mM KCl, 1.5 mM $MgCl_2$, 1 mM EDTA, 1 mM EGTA and 1 mM DTT) containing protease inhibitor cocktail. Cells were homogenized with a 25-gauge syringe needle on ice. The lysate was centrifuged at 1,000*g* for 5 min; the pellet was designated the nuclear fraction. The postnuclear supernatant was centrifuged at 6,000*g* for 5 min to remove the mitochondrial fraction. The 6,000*g* supernatant was subjected to centrifugation at 20,000*g* for 2 h; the pellet was designated the membrane fraction. The 20,000*g* supernatant was designated the cytosol fraction. All fractions were dissolved in 4% SDS lysis buffer (4% SDS, 50 mM triethanolamine pH 7.4 and 150 mM NaCl). Equivalent portions of different fractions were then subjected to western blot analyses.

Immunofluorescence

Cells were seeded in 35-mm glass bottom dishes (MatTek) and fixed with 4% paraformaldehyde (v/v in PBS) for 30 min. The fixed cells were washed twice with PBS, permeabilized and blocked with 0.1% saponin/5% BSA/PBS for 30 min. The permeabilized cells were incubated overnight at 4 °C in the dark with primary antibody, followed by incubation with secondary antibody at RT in the dark for 1 h. Samples were mounted with Fluoromount-G (0100–01, SouthernBiotech) or DAPI Fluoromount-G (0100–20, SouthernBiotech) and observed using inverted confocal microscopy (LSM880, Zeiss).

qPCR

For the gene expression analysis, the qPCR was performed using SYBR Green PCR Master Mix according to the manufacturer's standard protocol. Primer sequences were from refs. [28–30].

Flow cytometry analysis

For FACS analysis, flow cytometry was performed using 1×10^6 cells per sample. The T_H17 cells were stimulated with cytokines cocktail: 3 ng ml^{-1} TGF-β (100–21, PeproTech), 40 ng ml^{-1} IL-6 (200–06, PeproTech), 30 ng ml^{-1} IL-23 (200–23, PeproTech), 20 ng ml^{-1} TNF (300–01A, PeproTech) and 10 ng ml^{-1} IL-1β (200–01B, PeproTech), and then labelled with Cy5.5-CD4 (560767, BD Pharmingen). After permeabilization and fixation, the cells were

labelled with PE-IL-17 (560767, BD Pharmingen). The cells were detected by Attune Flow Cytometer (Thermo Fisher) and analysed with FCS Express 6 software (De Novo Software).

Statistical analysis

Quantitative analyses were performed with SPSS 17.0 and data was expressed as mean ± s.e.m.. Comparisons among groups were performed using Student's *t*-test and other data were analysed using a one-way analysis of variance (ANOVA).

Reporting summary

Further information on research design is available in the Nature Research Reporting Summary linked to this paper.

Data availability

The main data supporting the findings of this study are available within the Article and its Supplementary Information. Raw data gels are in Supplementary Fig. 1 and statistical and reproducibility information can be found in the Supplementary Information. Additional data are available from the corresponding author upon reasonable request.

Extended Data

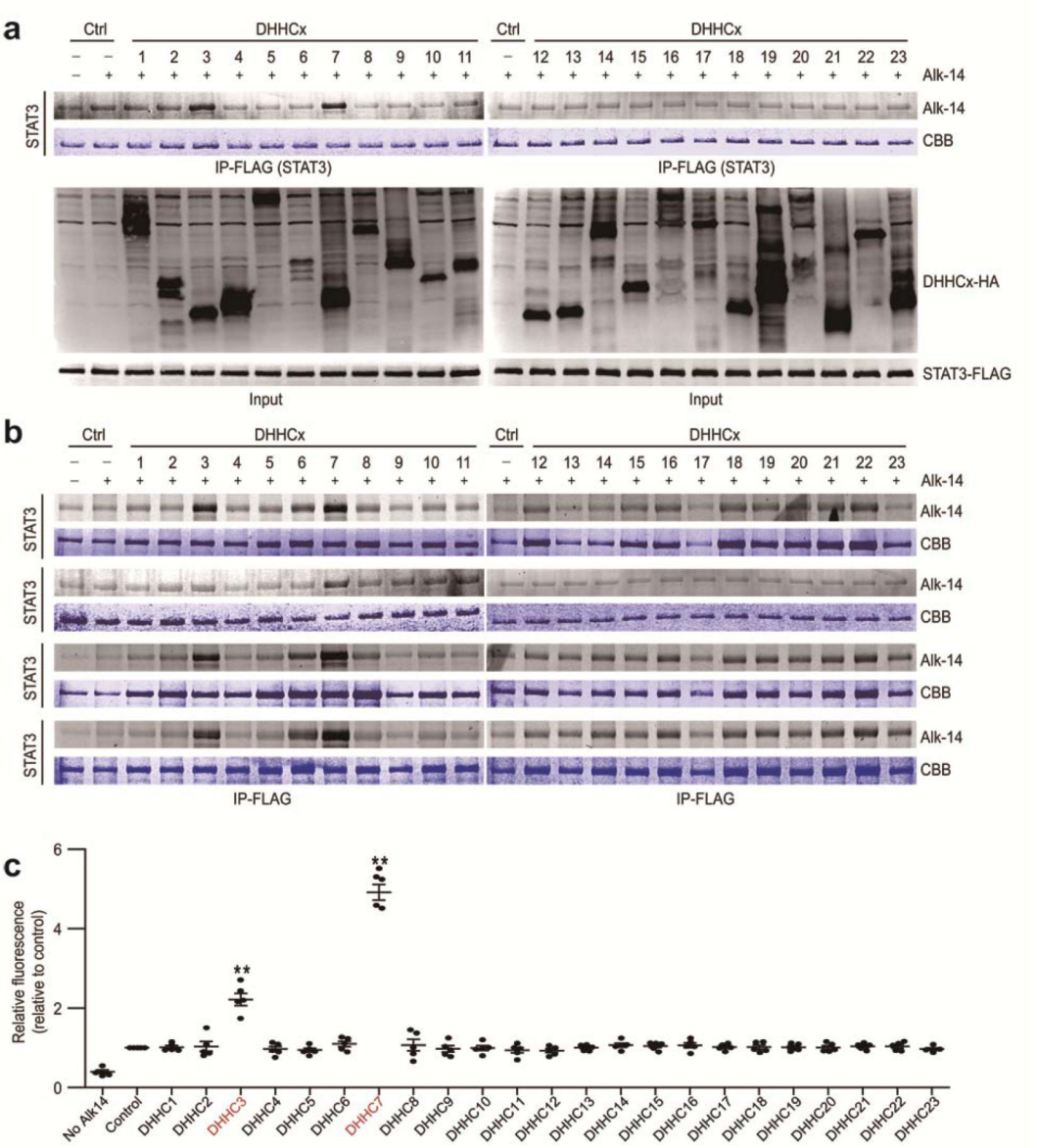

Extended Data Fig. 1 |. DHHC7 and DHHC3 are the palmitoyltransferases for STAT3.

a, **b**, HEK293T cells were transfected with Flag–STAT3 and HA–DHHC1–23 plasmid to screen for DHHCs that could increase STAT3 palmitoylation. The palmitoylation level was detected using Alk14 metabolic labelling, click chemistry to install a fluorescent tag, and in-gel fluorescence. The DHHC proteins analysed were from mice, and the protein number corresponds to the gene number with the exception of DHHC10/*Zdhhc11*, DHHC11/*Zdhhc23*, DHHC13/*Zdhhc24*, DHHC22/*Zdhhc13* and DHHC24/*Zdhhc22* (ref. [22]). **b** shows multiple replicates. **c**, Quantification of the relative palmitoylation levels in **a** and **b**. The palmitoylation level was normalized by STAT3 protein level and the level of negative control (with Alk14 but without DHHC overexpression) was set to 1. Quantification data are expressed as mean ± s.e.m. $^{**}P < 0.01$.

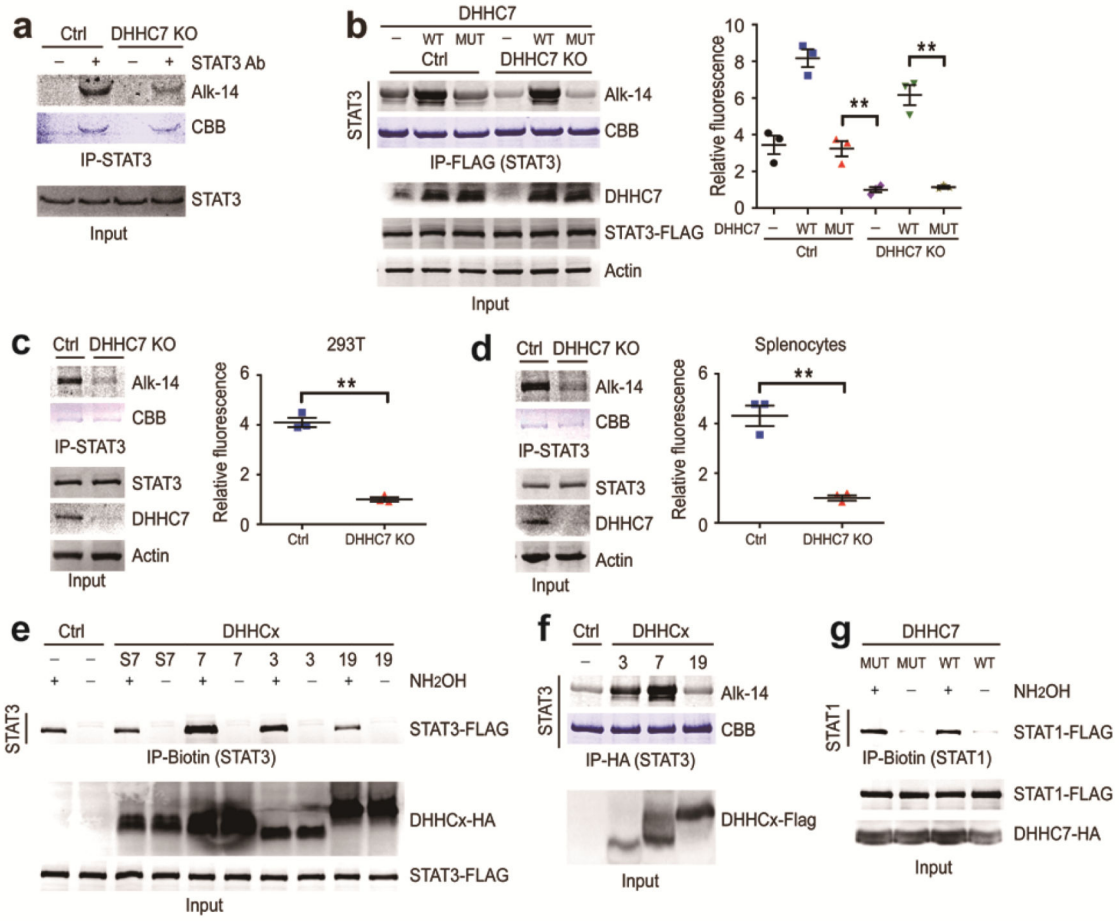

Extended Data Fig. 2 |. DHHC7 is the major palmitoyltransferase for STAT3.

a, Endogenous STAT3 palmitoylation in wild-type and DHHC7-knockout HEK293T cells determined using Alk14 labelling. **b**, Wild-type (WT) and DHHC7-knockout (MUT) HEK293T cells were transfected with DHHC7 or DHHS7 and labelled with Alk14. The palmitoylation level of overexpressed STAT3 was detected by in-gel fluorescence (left). The relative palmitoylation level was quantified (right). **c**, **d**, Endogenous STAT3 palmitoylation in wild-type and DHHC7-knockout HEK293T cells (**c**) and splenocytes from the DSS-induced colitis mice (**d**) determined using Alk14 labelling. The palmitoylation level of STAT3 was detected by in-gel fluorescence (left) and quantified (right). **e**, ABE method confirming DHHC7 as the major enzyme that promotes STAT3 palmitoylation. HEK293T cells were transfected with Flag–STAT3 and different HA–DHHC (mouse) plasmids. The pulled-down STAT3 with or without NH_2OH treatment was detected by western blot. **f**, HEK293T cells were transfected with HA-tagged STAT3 and Flag-tagged human DHHC3/7/19 to confirm that human DHHC7 could increase STAT3 palmitoylation. Palmitoylation level was detected using Alk14 metabolic labelling, click chemistry to install a fluorescent tag and in-gel fluorescence. **g**, DHHC7 expression does not affect STAT1 palmitoylation. HEK293T cells were transfected with Flag–STAT1 and different HA–DHHC7 plasmids. The palmitoylation level of STAT1 was detected using ABE. Quantification data are mean ± s.e.m. $^{**}P < 0.01$.

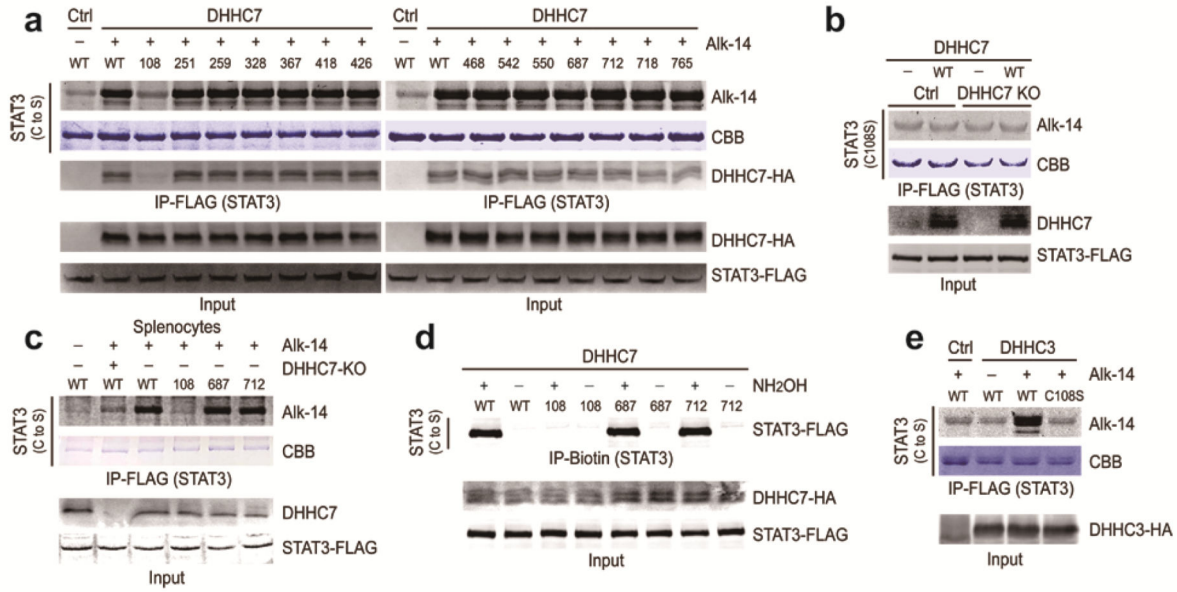

Extended Data Fig. 3 |. STAT3 is palmitoylated at Cys108.

a, HEK293T cells were transfected with HA–DHHC7 and different Flag–STAT3 mutants and labelled with Alk14. The palmitoylation levels of immunoprecipitated STAT3 were visualized by in-gel fluorescence. Co-immunoprecipitated DHHC7-HA was blotted. **b**, The mutant STAT3(C108S) could not be palmitoylated by DHHC7. Wild-type and DHHC7-knockout HEK293T cells were transfected with the indicated plasmids and treated with Alk14. The palmitoylation level of immunoprecipitated STAT3(C108S) was visualized by in-gel fluorescence. **c**, Wild-type and DHHC7-knockout mouse splenocytes were transfected with different Flag–STAT3 mutants and labelled with Alk14. The palmitoylation levels of immunoprecipitated STAT3 were visualized by in-gel fluorescence. **d**, Palmitoylation of wild-type STAT3 and mutants detected using the ABE method. HEK293T cells were transfected with HA–DHHC7 and different Flag–STAT3 mutants. **e**, DHHC3 expression can increase STAT3 C108 palmitoylation. HEK293T cells were transfected with Flag–STAT3 and HA–DHHC3 plasmids and labelled with Alk14. The fatty acylation level of STAT3 was detected by in-gel fluorescence.

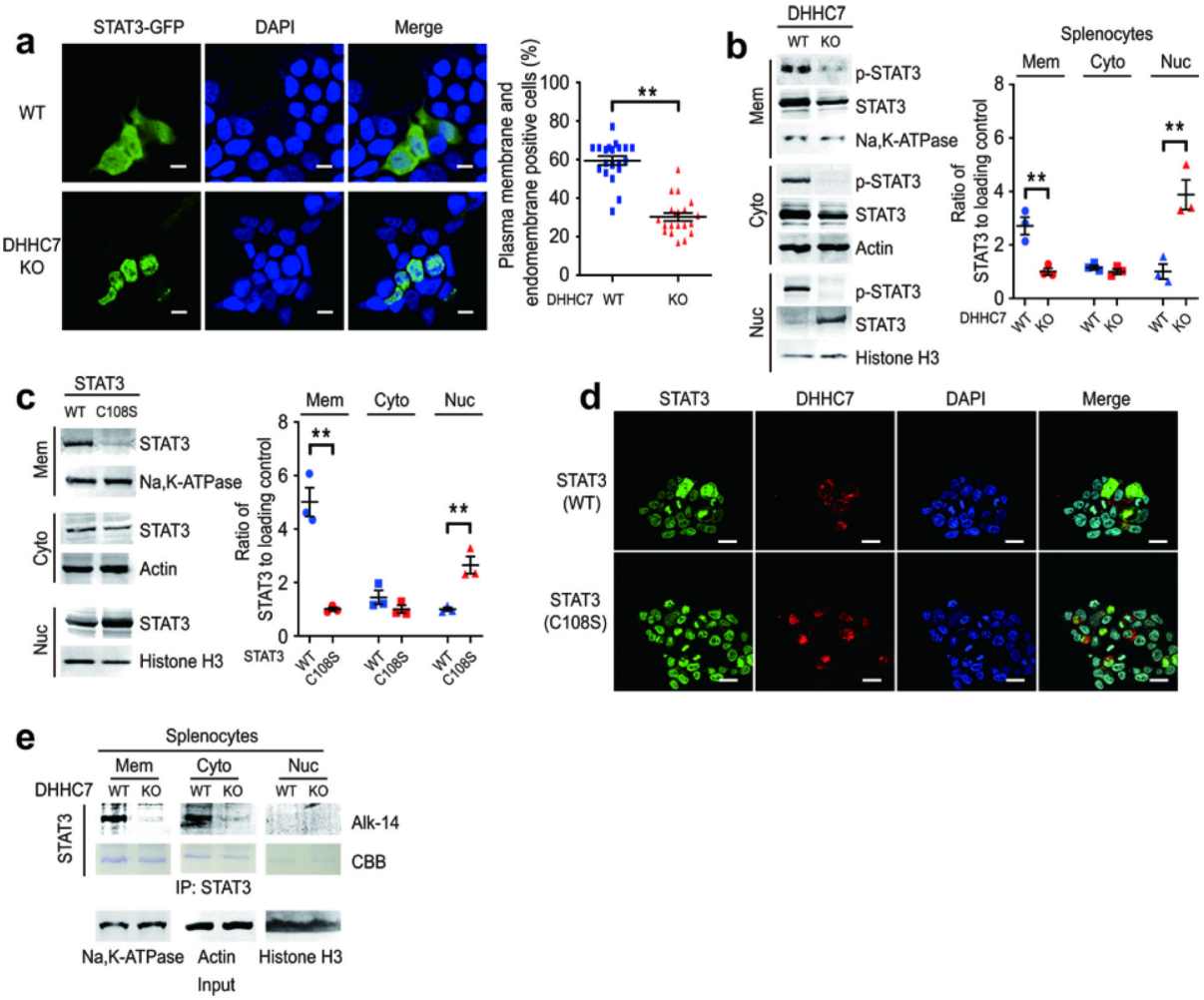

Extended Data Fig. 4 |. STAT3 C108 palmitoylation promotes STAT3 membrane localization.
a, The subcellular localization of EGFP-tagged STAT3 in wild-type and DHHC7-knockout HEK293T cells (left) was examined by confocal imaging. The percentage of cells with STAT3 plasma membrane and endomembrane was quantified (right). Scale bars, 50 μm. **b**, DHHC7 knockout decreases STAT3 membrane localization and increases its nuclear localization. Subcellular fractionation was carried out using wild-type and DHHC7-knockout splenocytes. Equivalent amounts of the nuclear and membrane fractions were then analysed by western blots (left). The relative STAT3 levels were quantified (right). Mem, membrane fraction; cyto, cytoplasmic fraction; nuc, nuclear fraction. **c**, STAT3(C108S) mutation decreases STAT3 membrane localization and increases nuclear localization. DHHC7-knockout HEK293T cells were transfected with HA–DHHC7 and the indicated Flag–STAT3 constructs and subcellular fractionation was performed. Equivalent amounts of the nuclear and membrane fractions were then analysed by western blot (left). The relative STAT3 levels were quantified (right). **d**, Confocal imaging showing the subcellular localization of EGFP-STAT3 (wild type) and EGFP-STAT3(C108S) in DHHC7-knockout HEK293T cells ectopically expressing DHHC7. Scale bars, 100 μm. **e**, STAT3 palmitoylation in different subcellular fractions of wild-type and DHHC7-knockout HEK293T cells. The cells were transfected with Flag–STAT3 and labelled with Alk14. Cell

fractionation was performed and the protein level of STAT3 was readjusted using Coomassie Brilliant Blue to ensure the equal loading of STAT3 in wild-type and knockout cell fractions for the gel analysis. The palmitoylation levels of immunoprecipitated STAT3 in the membrane, cytoplasmic and nuclear fractions were visualized by in-gel fluorescence. Quantification data are expressed as mean ± s.e.m. $^{**}P < 0.01$.

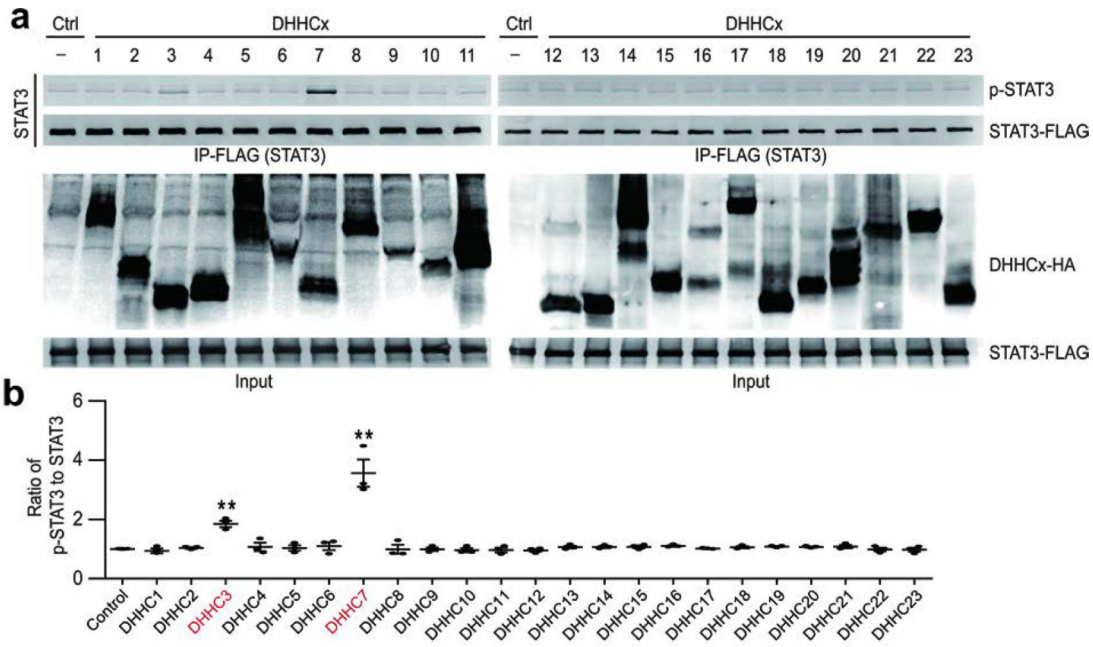

Extended Data Fig. 5 |. DHHC7 and DHHC3 promotes STAT3 phosphorylation.

a, Phosphorylation levels of Flag–STAT3 in HEK293T cells expressing HA-tagged mouse DHHC1–23. STAT3 was pulled down with Flag beads and subjected to western blot analyses. **b**, Quantification of the relative phosphorylation levels in **a**. The phosphorylation level was normalized to the STAT3 protein level and the level of the negative control was set to 1. Quantification data are expressed as mean ± s.e.m. $^{**}P < 0.01$.

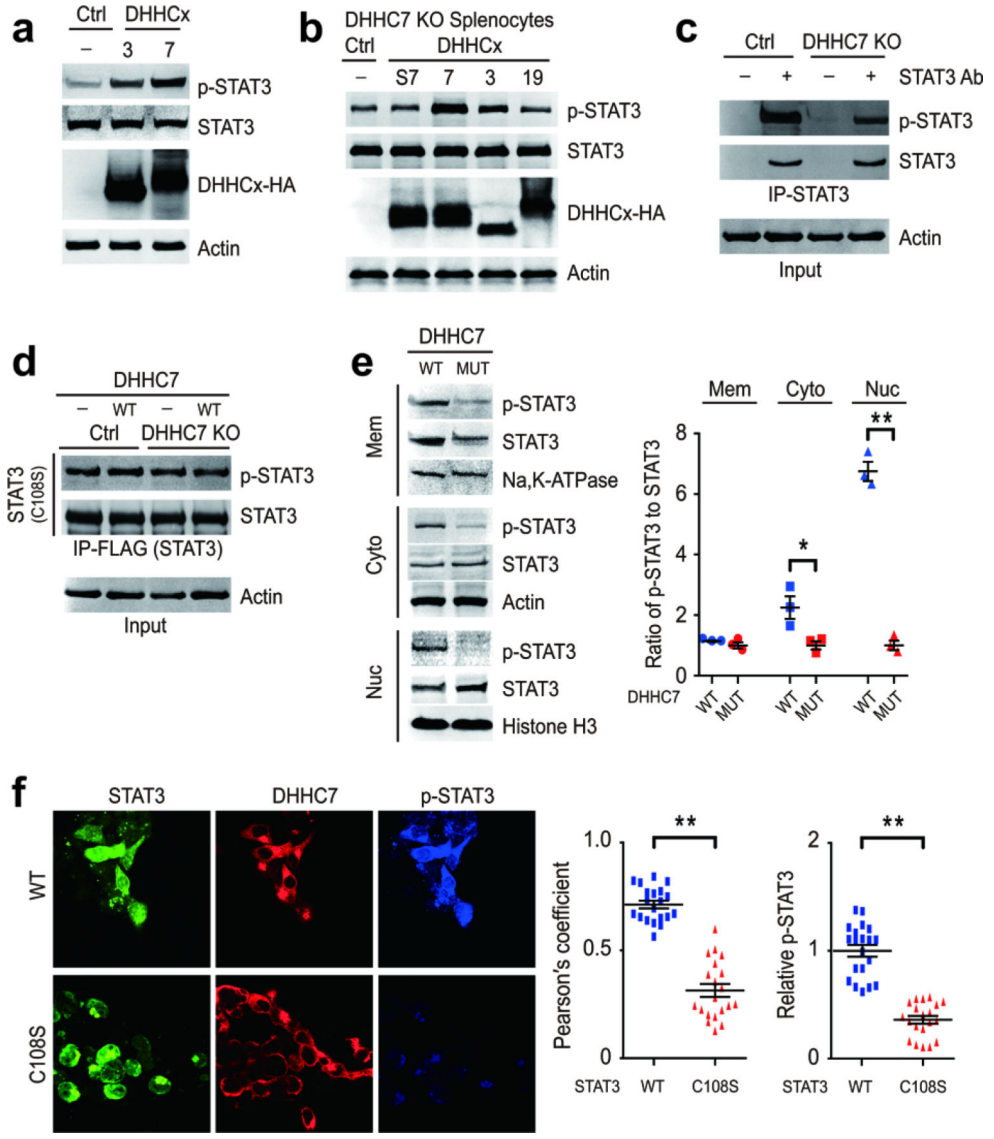

Extended Data Fig. 6 |. Palmitoylation promotes STAT3 phosphorylation.

a, DHHC3 and DHHC7 expression increases endogenous STAT3 phosphorylation in HEK293T cells. HEK293T cells were transfected with HA–DHHC3 and HA–DHHC7. The cells were lysed and subjected to western blot analyses as indicated. **b**, DHHC7 and DHHC3 expression in mouse splenocytes increased endogenous STAT3 phosphorylation. Mouse splenocytes were transfected with different HA–DHHCs and catalytically inactive DHHS7. The cells were lysed and subjected to western blot analyses as indicated. **c**, DHHC7 knockout in HEK293T cells decreased endogenous STAT3 phosphorylation. Cells were treated with Alk14, lysed, and STAT3 was immunoprecipitated with STAT3 antibody and protein A/G magnetic beads. Immunoprecipitated samples were analysed by western blot. **d**, The phosphorylation of STAT3(C108S) could not be promoted by DHHC7. Wild-type and DHHC7-knockout cells were transfected with indicated HA–DHHC7 and Flag–STAT3 plasmids. STAT3 was immunoprecipitated with Flag beads and analysed by western blot. **e**, Distribution of STAT3 and p-STAT3 in subcellular fractions of DHHC7-knockout HEK293T

cells reintroduced with DHHC7 or catalytically inactive DHHS7 (left). The relative p-STAT3 levels were quantified (right). **f**, The subcellular localization of STAT3 and p-STAT3 was analysed using confocal imaging after EGFP–STAT3 constructs and HA-tagged DHHC7 were transfected into DHHC7-knockout HEK293T cells. Co-localization of STAT3 and DHHC7 was analysed using Pearson's coefficient. The level of p-STAT3 was quantified. Scale bars, 100 μm. Quantification data are mean ± s.e.m. *$P < 0.05$; **$P < 0.01$.

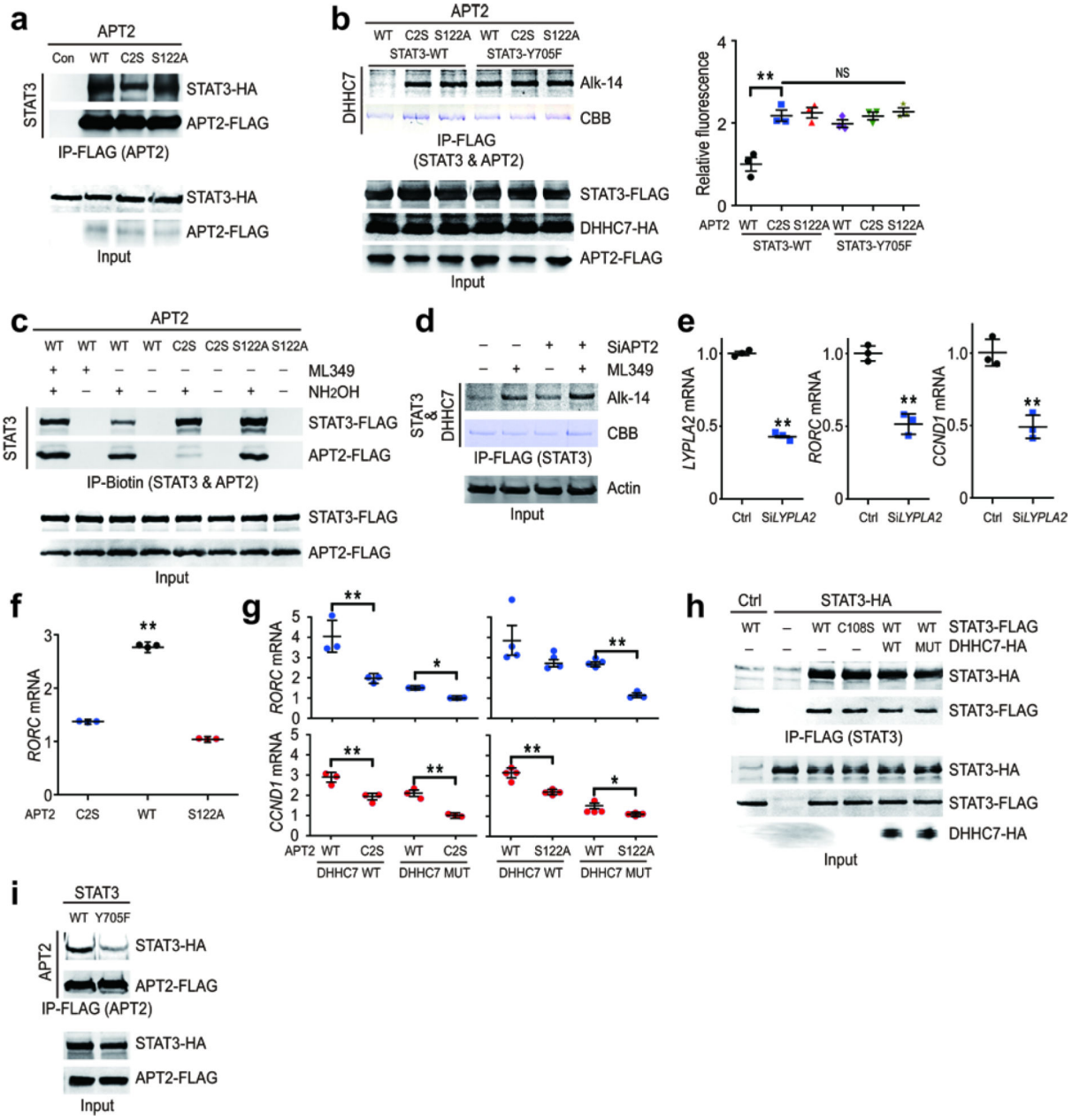

Extended Data Fig. 7 |. APT2 depalmitoylates STAT3 and promotes the nuclear translation of p-STAT3.

a, Flag–APT2 pulled down HA–STAT3 when co-expressed in HEK293T cells. The interaction of HA–STAT3 with Flag–APT2(C2S) was much weaker. **b**, Wild-type APT2

could remove the DHHC7-introduced palmitoylation on wild-type STAT3 better than that on the Y705F mutant. DHHC7-knockout HEK293T cells were transfected with the indicated plasmids. The cells were labelled with Alk14 and the palmitoylation of STAT3 was determined by in-gel fluorescence (left). The relative palmitoylation levels were quantified (right). **c**, In HEK293T cells, overexpression of wild-type APT2—but not the C2S or S122A mutant—decreased the palmitoylation level of Flag–STAT3 as determined by ABE. ML349 treatment (20 μM for 36 h) also increased the palmitoylation level. **d**, APT2 inhibition or knockdown increases Flag–STAT3 palmitoylation. DHHC7-knockout HEK293T cells were reintroduced with HA–DHHC7 and Flag–STAT3. Cells were then treated with siLYPLA2 or 20 μM of ML349 for 36 h before Alk14 labelling and in-gel fluorescence detection. **e**, *LYPLA2* siRNA knockdown in HEK293T cells decreased the mRNA levels of *RORC* and *CCND1*, two STAT3 target genes. **f**, Overexpression of Flag–APT2 (wild type), but not mutants, increased *RORC* mRNA levels in HEK293T cells. **g**, Co-expression of wild-type DHHC7 and APT2 strongly activated STAT3 signalling. DHHC7-knockout HEK293T cells were transfected with Flag–STAT3, different HA–DHHC7, and Flag–APT2 plasmids as indicated. The total mRNA was extracted and subjected to qPCR analysis of the indicated mRNA. **h**, STAT3 palmitoylation does not affect its dimerization. HEK293T cells were transfected with HA-tagged DHHC7, HA-tagged STAT3, and Flag-tagged STAT3. The level of Flag and HA-tagged STAT3 was determined after Flag-tag immunoprecipitation. **i**, Flag–APT2 interacted with HA–STAT3 (wild-type) better than it did with the Y705F mutant in HEK293T cells. Quantification data are mean ± s.e.m. $*P < 0.05$; $**P < 0.01$.

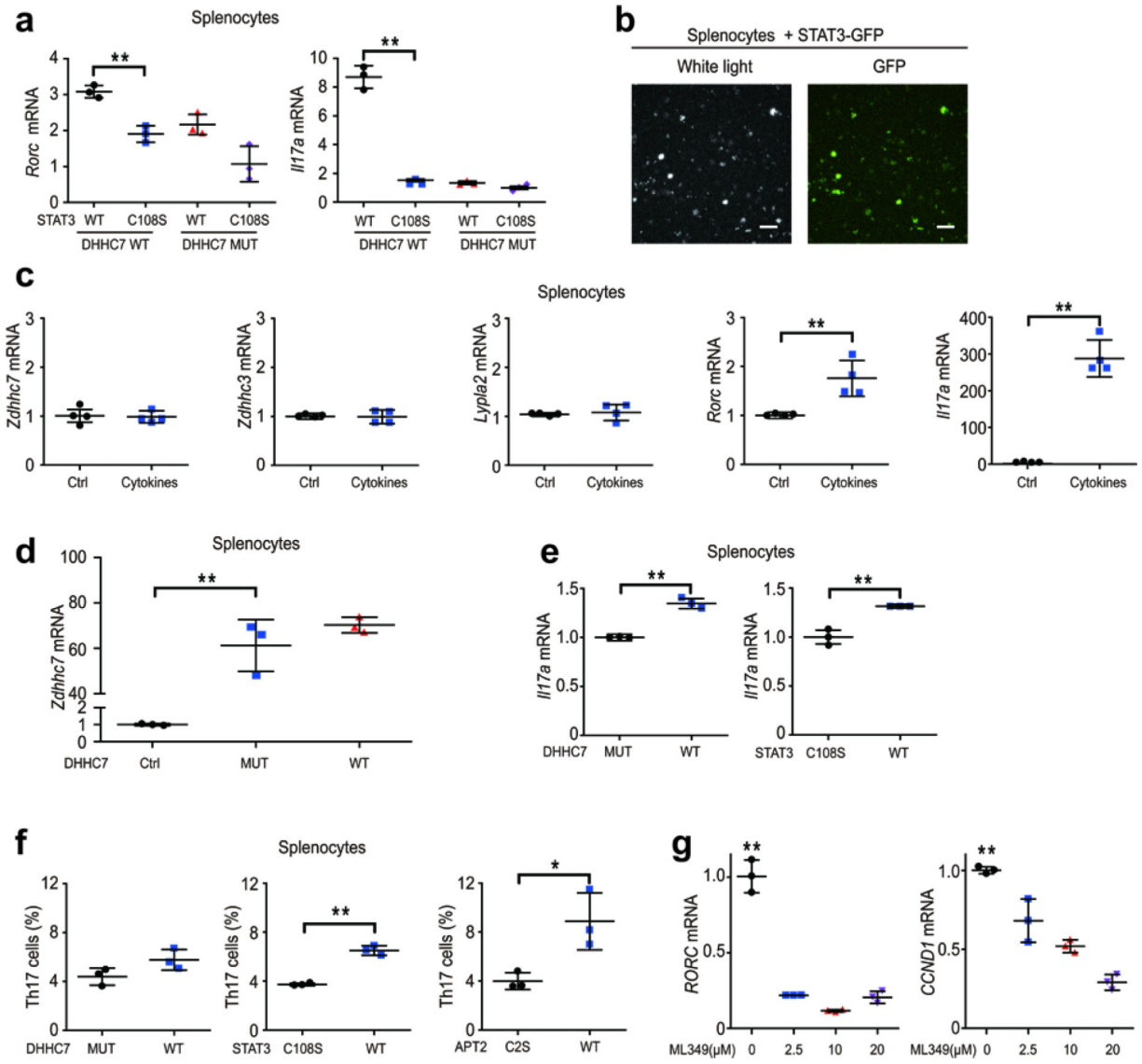

Extended Data Fig. 8 |. Expression of wild-type DHHC7 and APT2 in mouse splenocytes promotes T_H17 cell differentiation.

a, Co-expression of DHHC7 and STAT3 in splenocytes promotes T_H17 cell differentiation. Mouse splenocytes were transfected with different DHHC7 and STAT3 plasmids as indicated and then treated with a cytokine cocktail for 4 days to initiate differentiation. The *Rorc* and *Il17a* mRNA levels, markers for T_H17 differentiation, were analysed using qPCR. **b**, Splenocytes were transfected with EGFP-STAT3 plasmids and observed with confocal imaging. Scale bars, 100 μm. **c**, mRNA levels in splenocytes that were treated with a cytokine cocktail for 4 days to initiate differentiation. **d**, *ZDHHC7* mRNA levels were measured in splenocytes transfected with different DHHC7 and DHHS7 plasmids as indicated. **e**, *IL17A* mRNA levels were measured in splenocytes transfected with different plasmids as indicated. **f**, Mouse splenocytes were treated with a cytokine cocktail and transfected with different plasmids as indicated for 4 days, then the cells were collected and analysed by flow cytometry to detect CD4 and IL-17 positive cells (T_H17 cells). The

cytokine cocktail contains 3 ng ml^{-1} TGF-β, 40 ng ml^{-1} IL-6, 30 ng ml^{-1} IL-23, 20 ng ml^{-1} TNF and 10 ng ml^{-1} IL-1β. **g**, *RORC* and *CCND1* mRNA levels in HEK293T cells treated with the indicated concentrations of ML349 for 36 h. Quantification data are mean ± s.e.m. *$P < 0.05$; **$P < 0.01$.

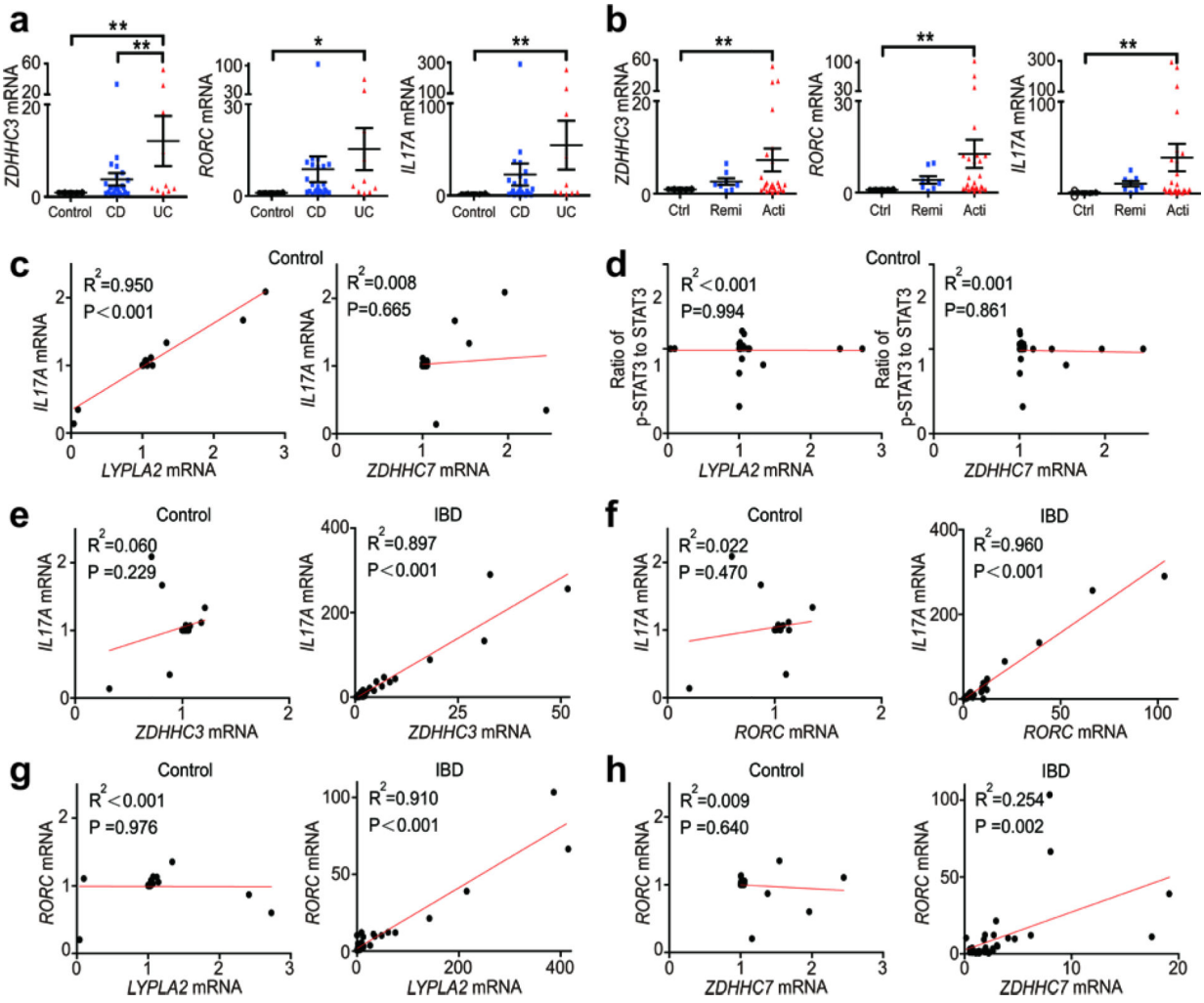

Extended Data Fig. 9 |. Human IBD patient gene expression data.

a, **b**, Human peripheral blood mononuclear cells (PBMCs) from 26 healthy participants, 24 patients with Crohn's disease (CD; 7 remission stage and 17 active stage) and 10 patients with ulcerative colitis (UC; 1 remission stage and 9 active stage) were extracted. The levels of *ZDHHC3* (we analysed *ZDHHC3* because DHHC3 also showed some activity towards STAT3), *RORC* and *IL17A* mRNA were analysed using qPCR. **c**, The correlation between *IL17A* and indicated mRNA levels in 26 healthy participants were analysed. **d**, The correlation between p-STAT3 and indicated mRNA levels in 26 healthy participants were analysed. **e**, The correlation between *ZDHHC3* and *IL17A* mRNA levels in 26 healthy participants and 34 patients with IBD (24 CD and 10 UC) were analysed. **f**, The correlation between *RORC* and *IL17A* mRNA levels in 26 healthy participants and 34 patients with IBD (24 CD and 10 UC) were analysed. **g**, The correlation between *LYPLA2* and *RORC*

mRNA levels in 26 healthy participants and 34 patients with IBD (24 CD and 10 UC) were analysed. **h**, The correlation between *ZDHHC7* and *RORC* mRNA levels in 26 healthy participants and 34 patients with IBD (24 CD and 10 UC) were analysed. Quantification data are mean ± s.e.m. **P* < 0.05; ***P* < 0.01.

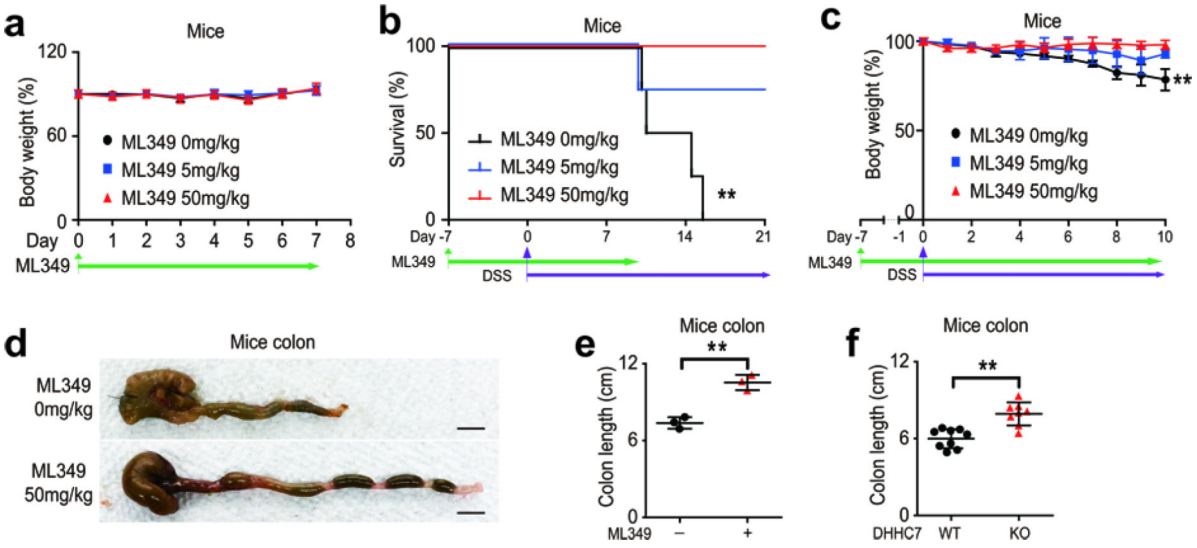

Extended Data Fig. 10 |. Mouse DSS model data.

a, ML349 toxicity study. C57BL/6J mice were intraperitoneally injected with ML349 for 7 days at the indicated doses and changes in body weight were evaluated. **b**, **c**, C57BL/6J mice were pretreated with daily ML349 intraperitoneal injections as indicated, then the ML349 treatment was combined with 2.5% DSS treatment in their drinking water ad libitum. Survival rate (**b**) and body weight changes (**c**) were evaluated. **d**, C57BL/6J mice were treated with 2.5% DSS treatment in their drinking water ad libitum and ML349 was injected daily intraperitoneally on the day that DSS treatment started. Colon morphology was evaluated at the end of the treatment. **e**, Quantitation of colon length shown in **d**. **f**, Wild-type and DHHC7-knockout mice were treated with 2.5% DSS in their drinking water ad libitum. Colon length was evaluated. Quantification data are mean ± s.e.m. ***P* < 0.01.

Supplementary Material

Refer to Web version on PubMed Central for supplementary material.

Acknowledgements

We thank W. Teng for help with replicating some APT2 experiments, and the Cornell University Biotechnology Resource Center (BRC) Imaging Facility for help with the confocal microscopy, which is supported by National Institutes of Health (NIH) grant S10RR025502. This work is supported in part by NIH grants R01GM121540 (to M.E.L.), R35GM131808 (to H.L.) and DK107868 (to H.L.), and by funds from the Howard Hughes Medical Institute and Cornell University.

References

1. Jiang H et al. Protein lipidation: occurrence, mechanisms, biological functions, and enabling technologies. Chem. Rev. 118, 919–988 (2018). [PubMed: 29292991]

2. Linder ME & Jennings BC Mechanism and function of DHHC S-acyltransferases. Biochem. Soc. Trans. 41, 29–34 (2013). [PubMed: 23356254]
3. Johnson DE, O'Keefe RA & Grandis JR Targeting the IL-6/JAK/STAT3 signalling axis in cancer. Nat. Rev. Clin. Oncol. 15, 234–248 (2018). [PubMed: 29405201]
4. Coskun M, Vermeire S & Nielsen OH Novel targeted therapies for inflammatory bowel disease. Trends Pharmacol. Sci. 38, 127–142 (2017). [PubMed: 27916280]
5. Britton GJ et al. Microbiotas from humans with inflammatory bowel disease alter the balance of gut T_H17 and $ROR\gamma t^+$ regulatory T cells and exacerbate colitis in mice. Immunity 50, 212–224.e4 (2019). [PubMed: 30650377]
6. Mangan PR et al. Transforming growth factor-β induces development of the T_H17 lineage. Nature 441, 231–234 (2006). [PubMed: 16648837]
7. Zhou L et al. *Faecalibacterium prausnitzii* produces butyrate to maintain T_H17/T_{reg} balance and to ameliorate colorectal colitis by inhibiting histone deacetylase 1. Inflamm. Bowel Dis. 24, 1926–1940 (2018). [PubMed: 29796620]
8. Dekker FJ et al. Small-molecule inhibition of APT1 affects Ras localization and signaling. Nat. Chem. Biol. 6, 449–456 (2010). [PubMed: 20418879]
9. Niu J et al. Fatty acids and cancer-amplified ZDHHC19 promote STAT3 activation through S-palmitoylation. Nature 573, 139–143 (2019); retraction 583, 154 (2020). [PubMed: 31462771]
10. Jing H et al. SIRT2 and lysine fatty acylation regulate the transforming activity of K-Ras4a. eLife 6, e32436 (2017). [PubMed: 29239724]
11. Verhoeven Y et al. The potential and controversy of targeting STAT family members in cancer. Semin. Cancer Biol. 60, 41–56 (2020). [PubMed: 31605750]
12. Carpenter RL & Lo HW STAT3 target genes relevant to human cancers. Cancers (Basel) 6, 897–925 (2014). [PubMed: 24743777]
13. Rocks O et al. An acylation cycle regulates localization and activity of palmitoylated Ras isoforms. Science 307, 1746–1752 (2005). [PubMed: 15705808]
14. Kong E et al. Dynamic palmitoylation links cytosol-membrane shuttling of acyl-protein thioesterase-1 and acyl-protein thioesterase-2 with that of proto-oncogene H-Ras product and growth-associated protein-43. J. Biol. Chem. 288, 9112–9125 (2013). [PubMed: 23396970]
15. Kathayat RS et al. Active and dynamic mitochondrial S-depalmitoylation revealed by targeted fluorescent probes. Nat. Commun. 9, 334 (2018). [PubMed: 29362370]
16. Hernandez JL et al. APT2 inhibition restores Scribble localization and S-palmitoylation in Snail-transformed cells. Cell Chem. Biol. 24, 87–97 (2017). [PubMed: 28065656]
17. Yuan ZL, Guan YJ, Chatterjee D & Chin YE STAT3 dimerization regulated by reversible acetylation of a single lysine residue. Science 307, 269–273 (2005). [PubMed: 15653507]
18. Klampfer L Signal transducers and activators of transcription (STATs): novel targets of chemopreventive and chemotherapeutic drugs. Curr. Cancer Drug Targets 6, 107–121 (2006). [PubMed: 16529541]
19. Mucida D et al. Reciprocal T_H17 and regulatory T cell differentiation mediated by retinoic acid. Science 317, 256–260 (2007). [PubMed: 17569825]
20. Minegishi Y et al. Molecular explanation for the contradiction between systemic T_H17 defect and localized bacterial infection in hyper-IgE syndrome. J. Exp. Med. 206, 1291–1301 (2009). [PubMed: 19487419]
21. Chen ZQ, Ulsh LS, DuBois G & Shih TY Posttranslational processing of p21 ras proteins involves palmitylation of the C-terminal tetrapeptide containing cysteine-186. J. Virol. 56, 607–612 (1985). [PubMed: 2997480]

References

22. Fukata Y, Iwanaga T & Fukata M Systematic screening for palmitoyl transferase activity of the DHHC protein family in mammalian cells. Methods 40, 177–182 (2006). [PubMed: 17012030]
23. Sandborn WJ et al. Phase II evaluation of anti-MAdCAM antibody PF-00547659 in the treatment of Crohn's disease: report of the OPERA study. Gut 67, 1824–1835 (2018). [PubMed: 28982740]

24. Krag A et al. Profermin is efficacious in patients with active ulcerative colitis—a randomized controlled trial. Inflamm. Bowel Dis. 19, 2584–2592 (2013). [PubMed: 24108114]

25. Liu H & Naismith JH An efficient one-step site-directed deletion, insertion, single and multiple-site plasmid mutagenesis protocol. BMC Biotechnol. 8, 91 (2008). [PubMed: 19055817]

26. Hsu PD et al. DNA targeting specificity of RNA-guided Cas9 nucleases. Nat. Biotechnol. 31, 827–832 (2013). [PubMed: 23873081]

27. Hurst CH, Turnbull D, Plain F, Fuller W & Hemsley PA Maleimide scavenging enhances determination of protein S-palmitoylation state in acyl-exchange methods. Biotechniques 62, 69–75 (2017). [PubMed: 28193150]

28. Ohno Y, Kihara A, Sano T & Igarashi Y Intracellular localization and tissue-specific distribution of human and yeast DHHC cysteine-rich domain-containing proteins. Biochim. Biophys. Acta 1761, 474–483 (2006). [PubMed: 16647879]

29. Cao N et al. A potential role for protein palmitoylation and zDHHC16 in DNA damage response. BMC Mol. Biol. 17, 12 (2016). [PubMed: 27159997]

30. Kuwata S et al. Extracellular lipid metabolism influences the survival of ovarian cancer cells. Biochem. Biophys. Res. Commun. 439, 280–284 (2013). [PubMed: 23973712]

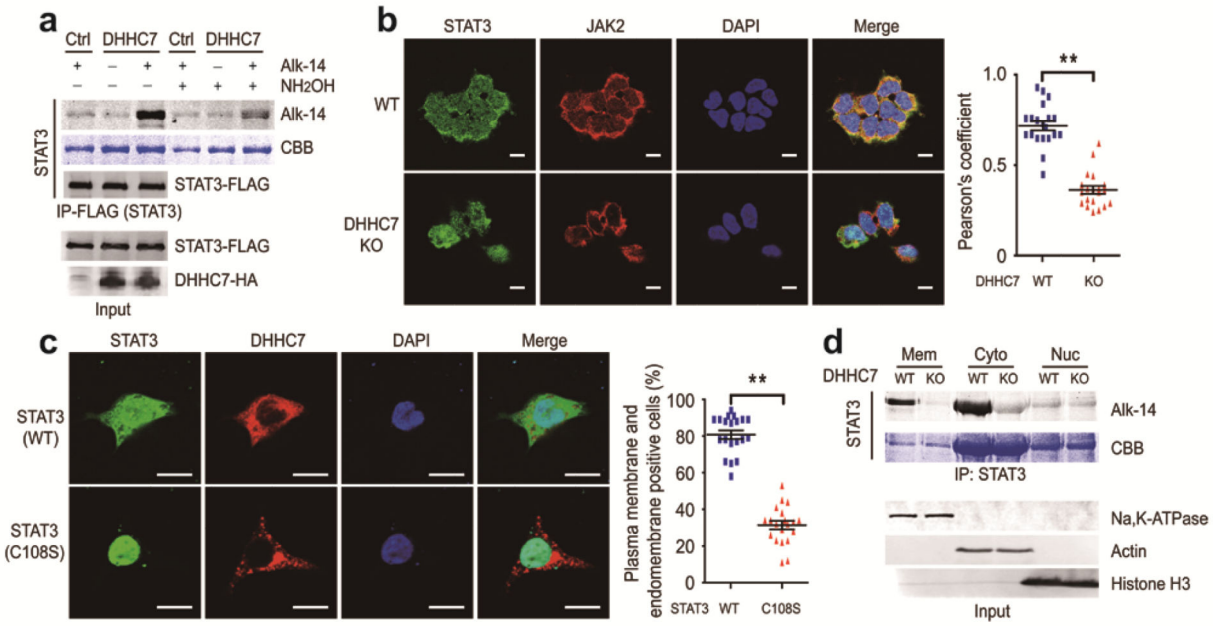

Fig. 1 |. DHHC7-induced palmitoylation promotes STAT3 membrane translocation.

a, HEK293T cells were transfected with Flag–STAT3 and HA–DHHC7. Palmitoylation levels of STAT3 with or without hydroxylamine (NH_2OH) treatment were detected using Alk14 labelling. **b**, Left, the subcellular localization of endogenous STAT3 and JAK2 was analysed using confocal imaging in wild-type and DHHC7-knockout HEK293T cells. Scale bars, 50 μm. Right, quantification of the colocalization of STAT3 and JAK2 using Pearson's correlation coefficients. **c**, Left, the subcellular localization of EGFP–STAT3 and EGFP–STAT3(C108S) in DHHC7 knockout HEK293T cells ectopically expressing DHHC7. Scale bars, 100 μm. Right, the percentage of DHHC7-positive cells in which STAT3 is translocated from the nucleus to the plasma membranes and endomembranes. **d**, Wild-type and DHHC7-knockout HEK293T cells were transfected with Flag–STAT3 and labelled with Alk14. Subcellular fractionation was performed and STAT3 protein levels were adjusted to ensure that there were equal amounts of STAT3 in the wild-type and knockout cell fractions used for the gel. The palmitoylation levels of immunoprecipitated STAT3 in the membrane (mem.), cytoplasmic (cyto.) and nuclear (nuc.) fractions were visualized by in-gel fluorescence. Data are mean ± s.e.m. $^{**}P < 0.01$. Raw data gels can be found in Supplementary Fig. 1 and statistical and reproducibility information can be found in the Supplementary Information.

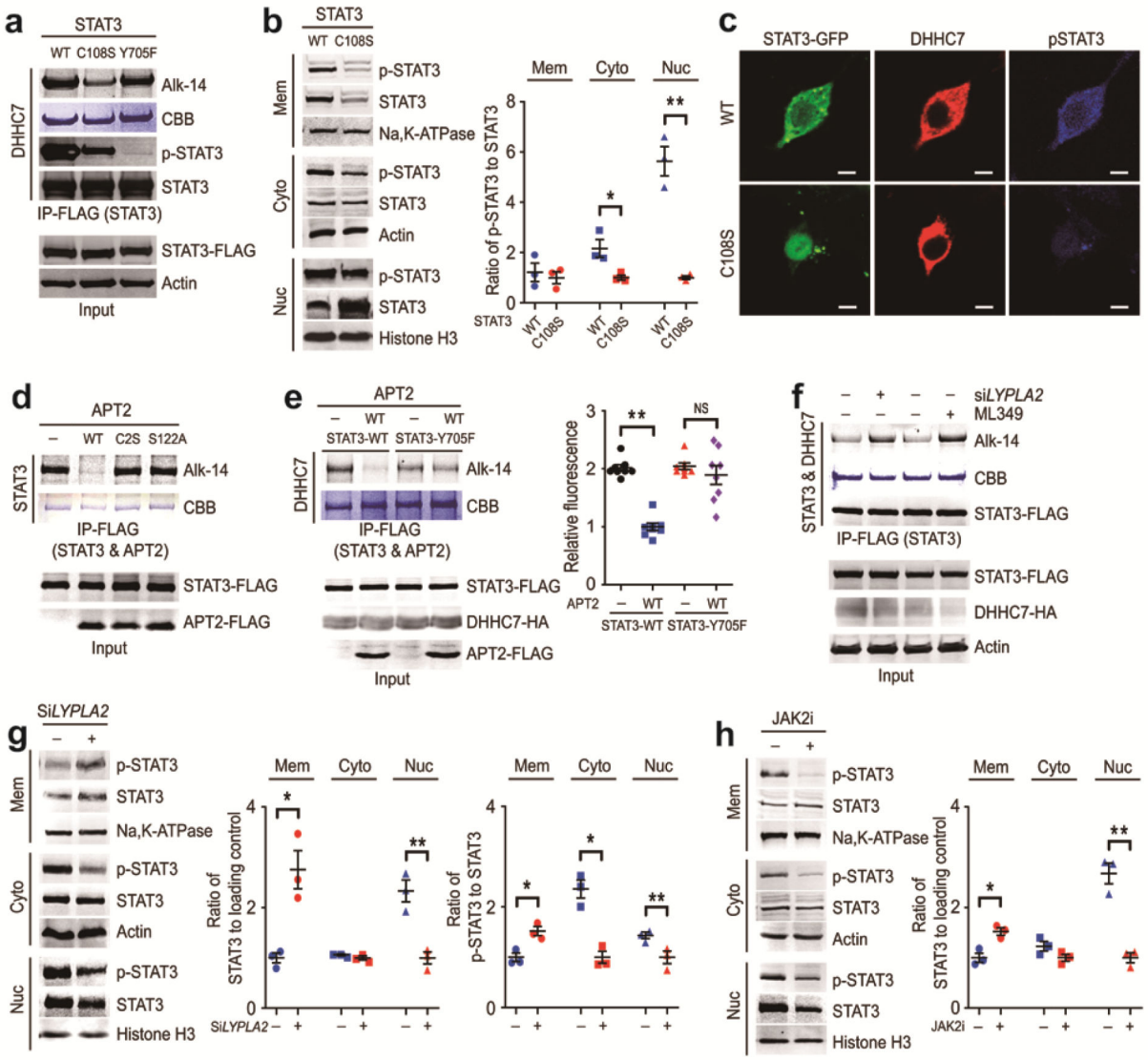

Fig. 2 |. APT2 is a depalmitoylase of STAT3 and palmitoylation/depalmitoylation promotes p-STAT3 nuclear localization.

a, C108 is the major palmitoylation site of STAT3. HEK293T cells were transfected with HA–DHHC7 and Flag–STAT3 (wild-type or mutants) and labelled with Alk14. STAT3 was pulled down and subjected to Alk14 labelling and western blot analyses. **b**, Left, distribution of wild-type or C108S mutants of STAT3 and p-STAT3 in the subcellular fractions of DHHC7-knockout HEK293T cells into which DHHC7 or DHHS7 were reintroduced. Right, quantification of the relative p-STAT3 levels. **c**, The subcellular localization of STAT3 and p-STAT3 was analysed using confocal imaging after different EGFP–STAT3 constructs and HA-tagged DHHC7 were transfected into DHHC7-knockout HEK293T cells. Scale bars, 50 μm. **d**, In HEK293T cells, overexpression of wild-type APT2—but not the C2S or S122A mutants—decreased the palmitoylation level of Flag–STAT3 as determined by Alk14 labelling. **e**, APT2 preferentially depalmitoylates wild-type STAT3 over the Y705F mutant. DHHC7-knockout HEK293T cells were transfected with the indicated plasmids and labelled

with Alk14. The palmitoylation of STAT3 was determined by in-gel fluorescence (left) and quantified (right). **f**, APT2 inhibition or knockdown increases the palmitoylation of Flag–STAT3. DHHC7-knockout HEK293T cells were reintroduced with HA–DHHC7 and Flag–STAT3, and treated with *LYPLA2* siRNA or 20 μM of ML349 for 36 h before Alk14 labelling and in-gel fluorescence detection. **g**, Left, distribution of STAT3 and p-STAT3 in different subcellular fractions of APT2-knockdown HEK293T cells. Right, quantification of the relative STAT3 and p-STAT3 levels in these fractions. **h**, Left, distribution of STAT3 and p-STAT3 in subcellular fractions of DHHC7-overexpressing HEK293T cells, with or without treatment with 1 μM of the JAK2 inhibitor fedratinib. Right, quantification of the relative STAT3 levels in these fractions. Data are mean ± s.e.m. $*P < 0.05$; $**P < 0.01$.

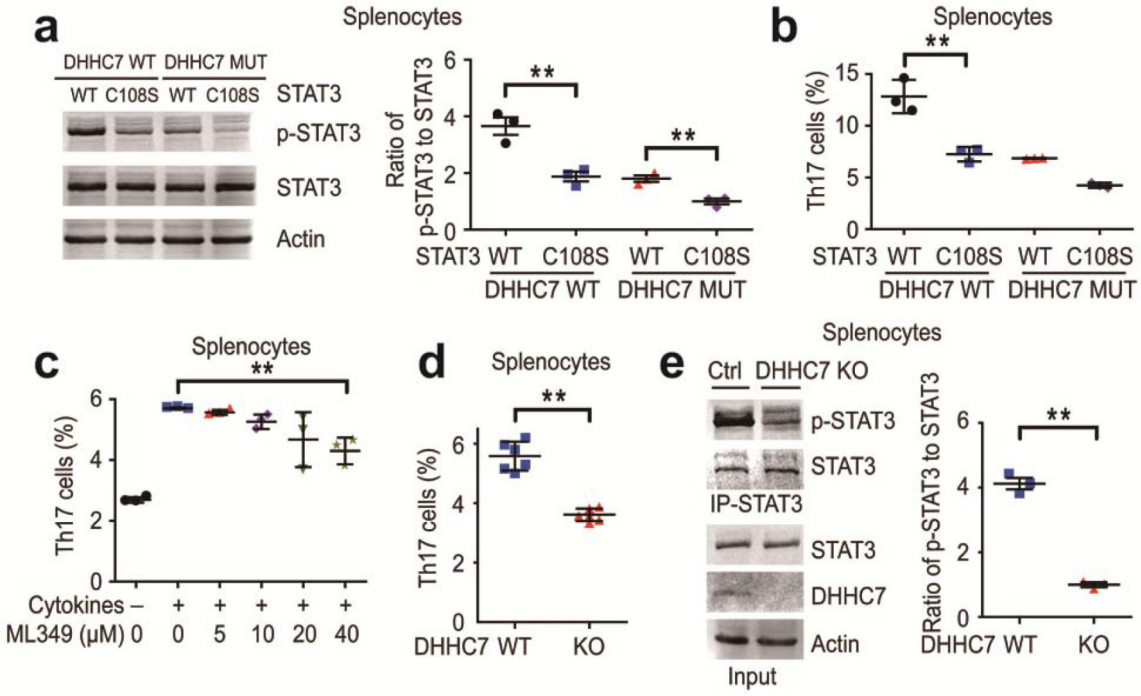

Fig. 3 |. The STAT3 palmitoylation–depalmitoylation cycle promotes T_H17 cell differentiation.
a, DHHC7 promotes phosphorylation of wild-type STAT3, but not of the C108S mutant, in mouse splenocytes. Left, STAT3 and p-STAT3 blots; right, quantification of the relative p-STAT3 levels. **b**, T_H17 cell differentiation was quantified in the splenocyte samples in **a** by flow cytometry. **c**, APT2 inhibition decreases T_H17 cell differentiation in a dose-dependent manner. Mouse splenocytes were treated with a cytokine cocktail (3 ng ml^{-1} TGF-β, 40 ng ml^{-1} IL-6, 30 ng ml^{-1} IL-23, 20 ng ml^{-1} TNF and 10 ng ml^{-1} IL-1β) and different concentrations of ML349 for 4 days, then collected and analysed by flow cytometry to detect CD4- and IL-17-positive cells. **d**, DHHC7 knockout in splenocytes inhibits T_H17 cell differentiation. Wild-type and DHHC7-knockout mouse splenocytes were treated with a cytokine cocktail for 4 days to initiate differentiation, then the cells were collected and analyse by flow cytometry to detect CD4- and IL-17-positive cells. **e**, Left, STAT3 and p-STAT3 blots of wild-type and DHHC7-knockout splenocytes. Right, quantification of the relative p-STAT3 levels. Data are mean ± s.e.m. $^{**}P < 0.01$.

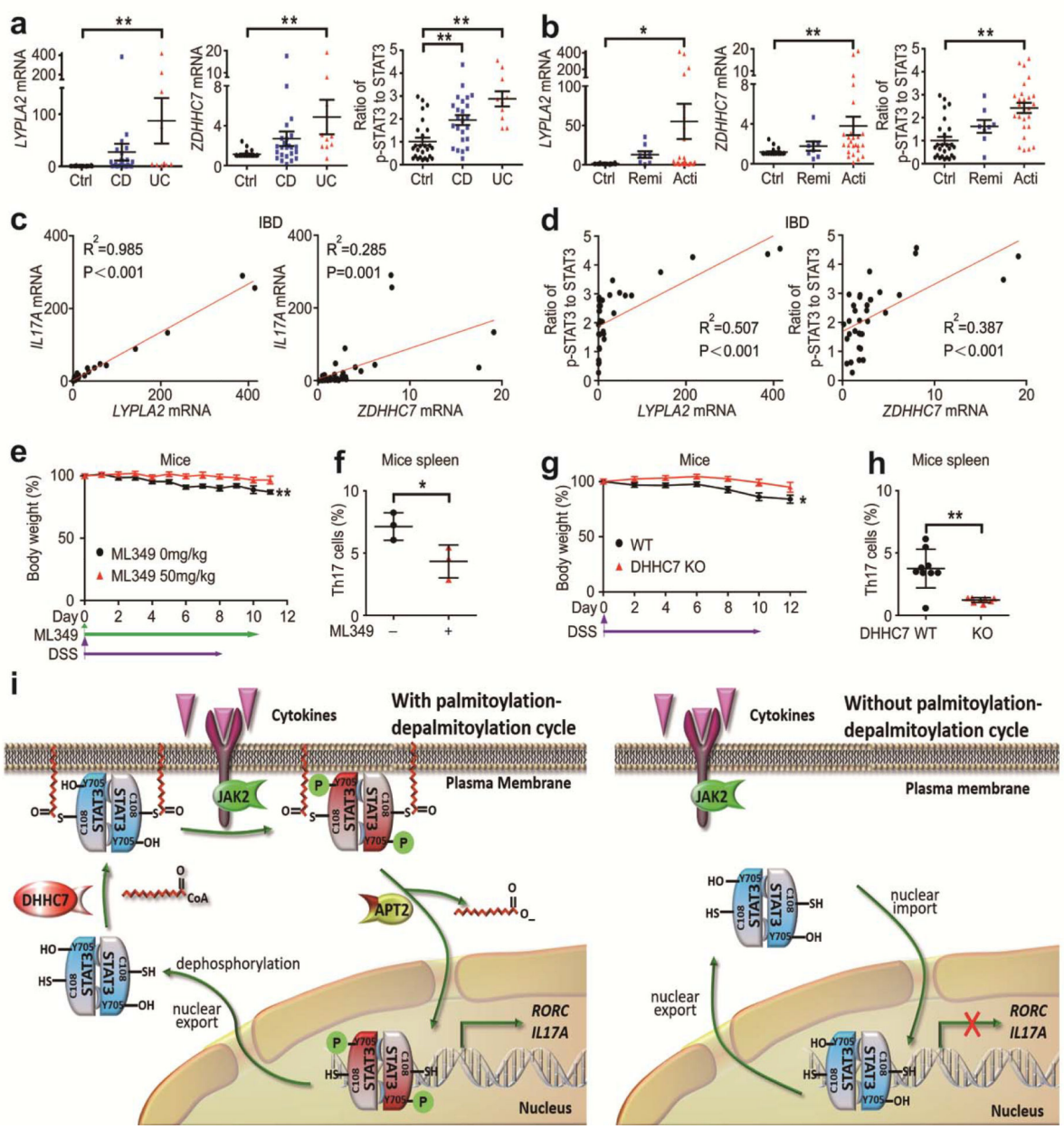

Fig. 4 |. The STAT3 palmitoylation–depalmitoylation cycle aggravates colitis.

a, **b**, Human PBMCs from 26 healthy participants (Ctrl), 24 patients with Crohn's disease (CD; 7 remission stage (rem.) and 17 active stage (act.)) and 10 patients with ulcerative colitis (UC; 1 remission stage and 9 active stage) were extracted. *LYPLA2* and *ZDHHC7* mRNA levels were analysed using qPCR. The relative p-STAT3 levels were quantified by western blots. **c**, **d**, The correlations between *IL17A* (**c**) or p-STAT3 (**d**) and the mRNA levels of the indicated genes in 34 patients with IBD. **e**, **f**, C57BL/6J mice were treated with 2.5% DSS in drinking water ad libitum and ML349 was intraperitoneally injected daily on the day that DSS treatment started. Body weight changes (**e**) and T_H17 cell levels in the spleen (**f**) were evaluated. **g**, **h**, Wild-type and DHHC7-knockout mice were treated with 2.5% DSS in drinking water ad libitum. Body weight changes (**g**) and T_H17 cell levels in the

spleen (**h**) were evaluated. **i**, Model of the regulation of STAT3 by the palmitoylation–depalmitoylation cycle. Palmitoylation of STAT3 by DHHC7 promotes the membrane recruitment and phosphorylation of STAT3. APT2 promotes the nuclear translocation of p-STAT3 by selectively depalmitoylating p-STAT3 over STAT3. The palmitoylation–depalmitoylation cycle drives the membrane localization and phosphorylation of STAT3, and the nuclear translocation of p-STAT3. The direction of the cycle is ensured by the preference of APT2 for p-STAT3 over STAT3. Data are expressed as the mean ± s.e.m. $*P < 0.05$; $**P < 0.01$.